LA-UR-19-30290
Approved for public release; distribution is unlimited.

Title:	Understanding Asteroid 16 Psyche's Composition through 3D Hydrocode Impact Crater Models
Author(s):	Caldwell, Wendy Kaye
Intended for:	Colloquium at University of Tennessee
Issued:	2019-10-10

Understanding Asteroid 16 Psyche's Composition through 3D Hydrocode Impact Crater Models

Wendy K. Caldwell

University of Tennessee Colloquium
October 11, 2019

wkcaldwell@lanl.gov

Los Alamos NATIONAL LABORATORY EST.1943

Managed by Triad National Security, LLC for the U.S. Department of Energy's NNSA

Impact Cratering

Dominant geologic process for solids in solar system

Types of impact craters:

- Simple
  - Diameter $<$ 3 km on Earth, $<$ 15 km on moon
  - Floor consists of breccia
  - Meteor Crater (Arizona)
- Complex
  - Diameter $>$ 3 km on Earth, $>$ 20 km on moon
  - Central peaks (collapsed bowl-shaped crater)
  - Floor has highly shocked and melted debris, melt pools sometimes
  - Flynn Creek Crater (Tennessee)
- Multiring basins
  - Diameter 100s to 1000s of km
  - Multiple concentric circular scarps

Stages of Impact Cratering

1. Contact and compression: transfer of energy and momentum, shock waves
2. Excavation: target material vaporized or ejected from crater, creating ejecta blanket
3. Modification: debris flows down toward center of crater (crater collapse)

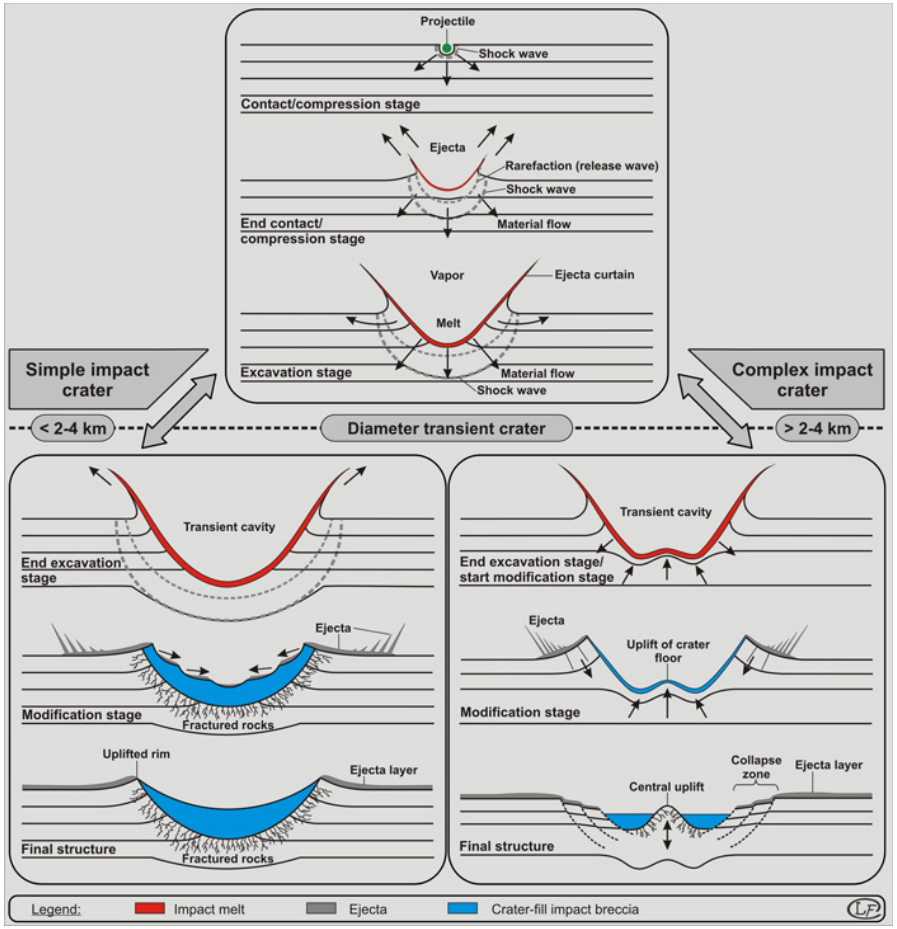

Image from http://www.meteorimpactonearth.com/mechanics.html.

174 Known Impact Structures on Earth

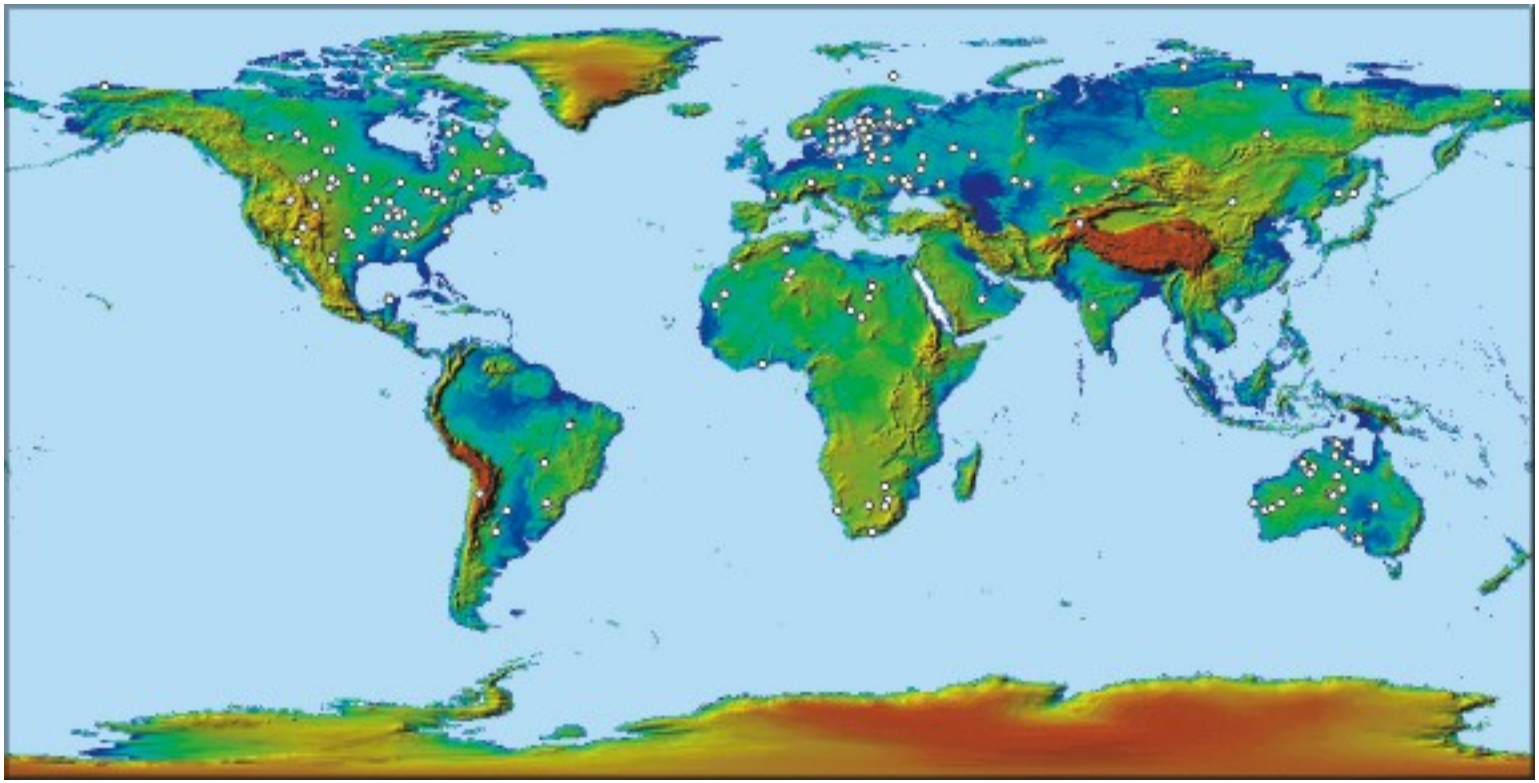

Image courtesy of University of New Brunswick Planetary and Space Science Center Earth Impact Database

Impacts Vary by Frequency and Energy

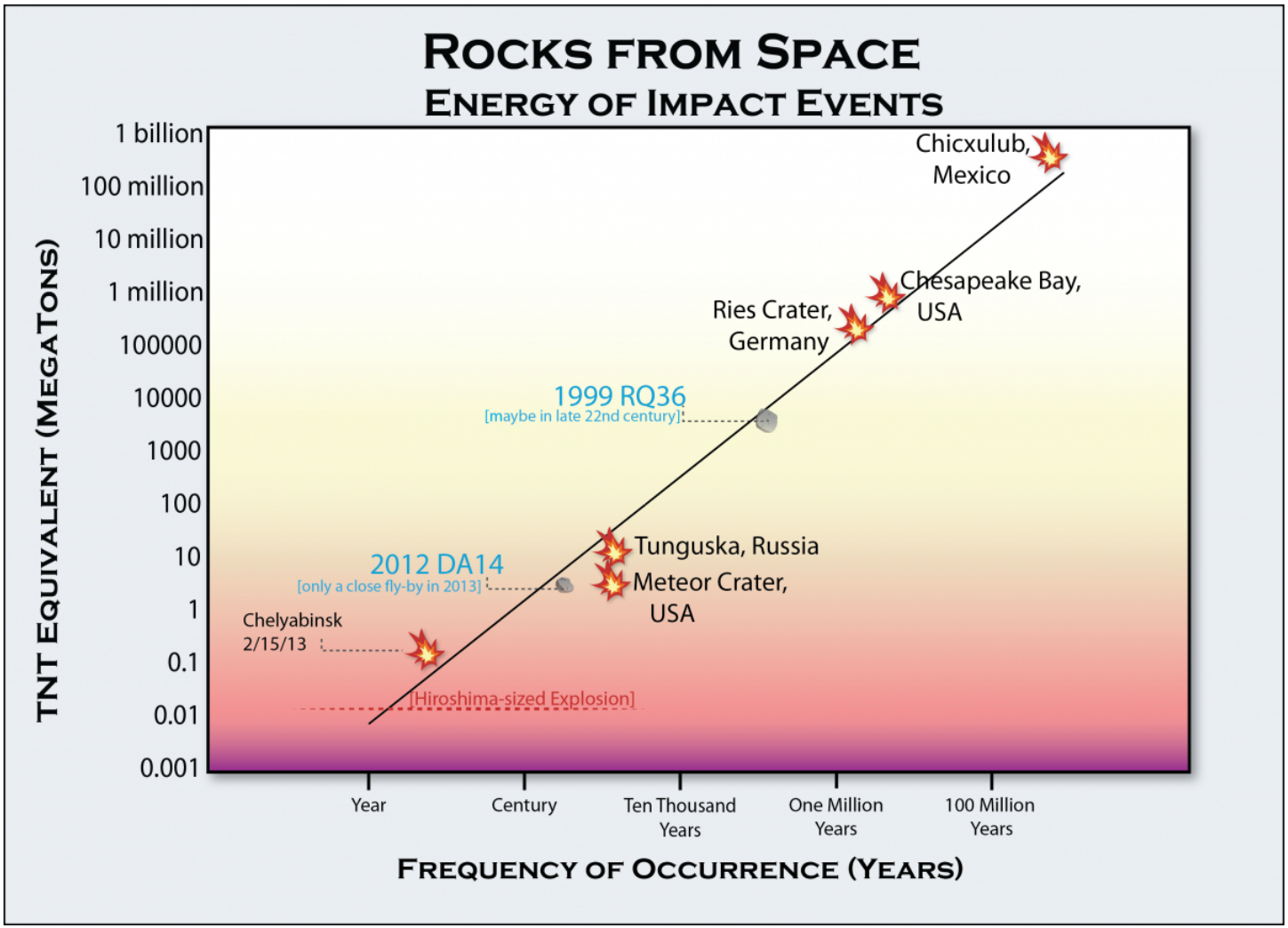

Image courtesy of LPL

Components of Hydrocode

Lagrangian forms of conservation of momentum (1), mass (2), energy(3):

$$\frac{\rho D\mathbf{u}}{Dt} = -\nabla P \quad (1)$$

$$\frac{D\rho}{Dt} + \rho\nabla \cdot \mathbf{u} = 0 \quad (2)$$

$$\frac{dE}{dt} + P\frac{dV}{dt} = 0, \quad (3)$$

D: Lagrangian differential $\left(\frac{\partial}{\partial t} + \mathbf{u}\cdot\nabla\right)$

EOS: relates pressure, density, internal energy

Constitutive model: stress tensor as a function of strain, strain rate effects, internal energy, damage

Hydrocode Methods and Approaches

Discretization Methods: finite-difference, finite element, Smooth Particle Hydrodynamics (SPH)

Approaches: Eulerian, Lagrangian, Arbitrary-Lagrangian-Eulerian (ALE)

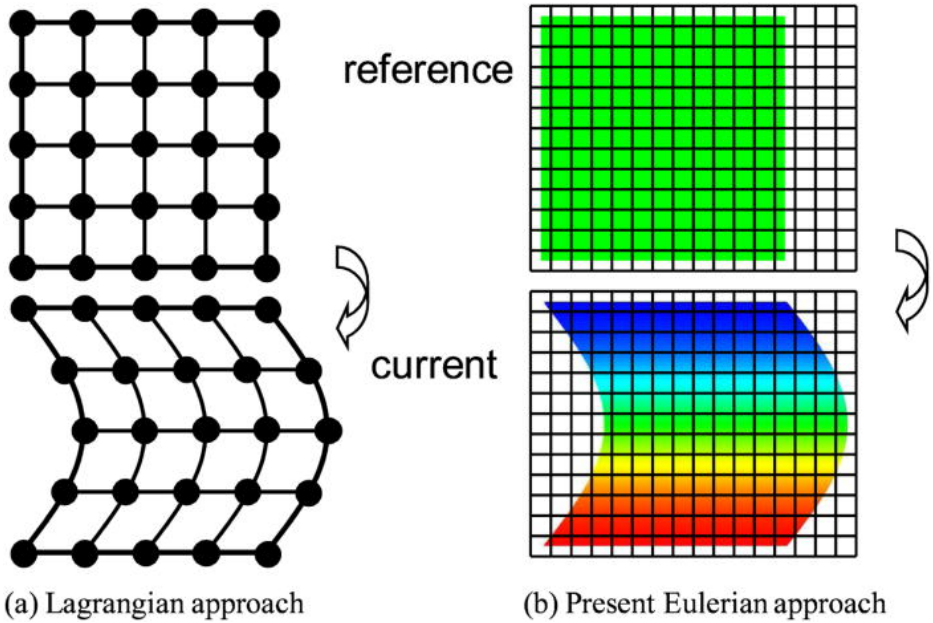

Image from
http://appliedmechanics.asmedigitalcollection.asme.org/article.aspx?articleid=1414433

Solid Mechanics and Damage

- Strength: ability to resist changing shape
- Strain: measure of deformation
- Stress: forces that cause deformation
- Elastic and plastic properties

Damage as an on/off switch

Image from
http://gamingrockson.blogspot.com/2012/09/top-5-worst-ways-to-die-in-super-mario.html

Damage Accumulates

Image from
https://i.ytimg.com/vi/AyYXWS61zEc/hqdefault.jpg

Constitutive Models

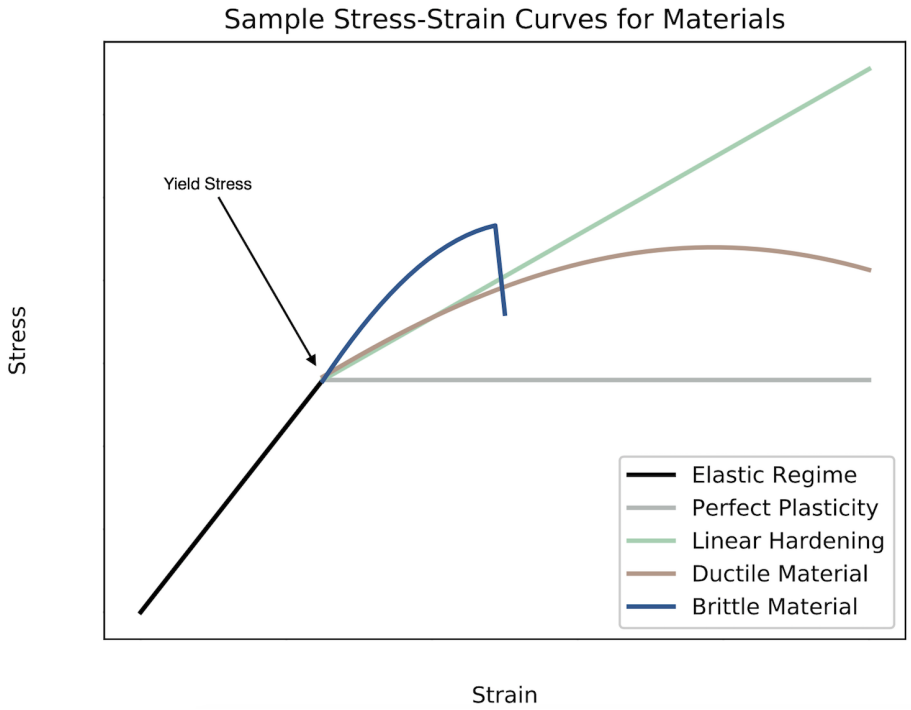

Figure: Sample stress-strain curves for perfectly plastic materials, materials that harden linearly, ductile materials, and brittle materials.

Perfect Plasticity[†]

$$\tau = \tau_y$$

Linear Hardening[†]

$$\tau = \tau_y + \bar{K}\epsilon$$

τ : flow stress (Pa)

τ_y : reference yield stress (Pa)

$\bar{K}$: hardening parameter

ϵ : equivalent plastic strain

[†] Simo, J. C. and T. J. R. Hughes. *Computational Inelasticity* Vol 7, Springer Science & Business Media (2006).

Constitutive Models

Johnson-Cook[†]

$$\tau = \underbrace{[A + B\epsilon^n]}_{\text{stress as function of strain}} \underbrace{\left[1 + C \ln\left(\hat{\dot{\epsilon}}\right)\right]}_{\text{strain rate effects}} \underbrace{\left[1 - \hat{T}^m\right]}_{\text{temperature effects}}$$

Steinberg-Guinan[‡]

$$G = G_0 \left[1 + \left(\frac{G'_P}{G_0}\right) \frac{P}{\eta^{\frac{1}{3}}} + \left(\frac{G'_T}{G_0}\right)(T - 300)\right]$$

$$\tau = \tau_y \left[1 + \beta\left(\epsilon + \epsilon_i\right)\right]^n \left[1 + \left(\frac{\tau'_P}{\tau_y}\right) \frac{P}{\eta^{\frac{1}{3}}} + \left(\frac{G'_T}{G_0}\right)(T - 300)\right]$$

[†] Johnson, G. R. and W. H. Cook. "A Constitutive Model and Data for Metals Subjected to Large Strains, High Strain Rates and High Temperatures," *Proceedings Seventh International Symposium on Ballistics* pp 541–547 (1983).

[‡] Steinberg, D., S. Cochran, and M. Guinan. "A constitutive model for metals applicable at high-strain rate," *Journal of Applied Physics* 51(3): 1498–1504 (1980).

Constitutive Models

Preston-Tonks-Wallace

$$G = G_0 \left(1 - \alpha \hat{T}\right)$$

Thermal Activation Regime

$$\hat{\tau}_s = s_0 - (s_0 - s_\infty) \operatorname{erf}\left[\kappa \hat{T} \ln\left(\frac{\gamma\dot{\xi}}{\dot{\epsilon}}\right)\right]$$

$$\hat{\tau}_y = y_0 - (y_0 - y_\infty) \operatorname{erf}\left[\kappa \hat{T} \ln\left(\frac{\gamma\dot{\xi}}{\dot{\epsilon}}\right)\right]$$

$$\hat{\tau} = \hat{\tau}_s + \frac{1}{p}\left(s_0 - \hat{\tau}_y\right) \ln\left\{1 - \left[1 - \exp\left(-p\frac{\hat{\tau}_s - \hat{\tau}_y}{s_0 - \hat{\tau}_y}\right)\right] \exp\left(-\frac{p\theta\epsilon}{\left(s_0 - \hat{\tau}_y\right)\left[\exp\left(p\frac{\hat{\tau}_s - \hat{\tau}_y}{s_0 - \hat{\tau}_y}\right) - 1\right]}\right)\right\}$$

Overdriven Shock Regime

$$\hat{\tau}_s = \max\left\{s_0 - (s_0 - s_\infty) \operatorname{erf}\left[\kappa \hat{T} \ln\left(\frac{\gamma\dot{\xi}}{\dot{\epsilon}}\right)\right], s_0\left(\frac{\dot{\epsilon}}{\gamma\dot{\xi}}\right)^\beta\right\}$$

$$\hat{\tau}_y = \max\left\{y_0 - (y_0 - y_\infty) \operatorname{erf}\left[\kappa \hat{T} \ln\left(\frac{\gamma\dot{\xi}}{\dot{\epsilon}}\right)\right], \min\left[y_1\left(\frac{\dot{\epsilon}}{\gamma\dot{\xi}}\right)^{y_2}, s_0\left(\frac{\dot{\epsilon}}{\gamma\dot{\xi}}\right)^\beta\right]\right\}$$

Preston, D. L., D. L. Tonks, and D. C. Wallace. “Model of plastic deformation for extreme loading conditions.” *Journal of Applied Physics* 93(1): 211–220 (2003).

Why Use FLAG to Model Impacts?

FLAG: A Big ASC Code

- Hydrodynamics code developed and maintained by LANL
- Arbitrary Lagrangian-Eulerian (ALE)
- Finite volume (conservative)
- Variety of Equations of State (EOS) and constitutive models
- Has been verified and validated for impact cratering†

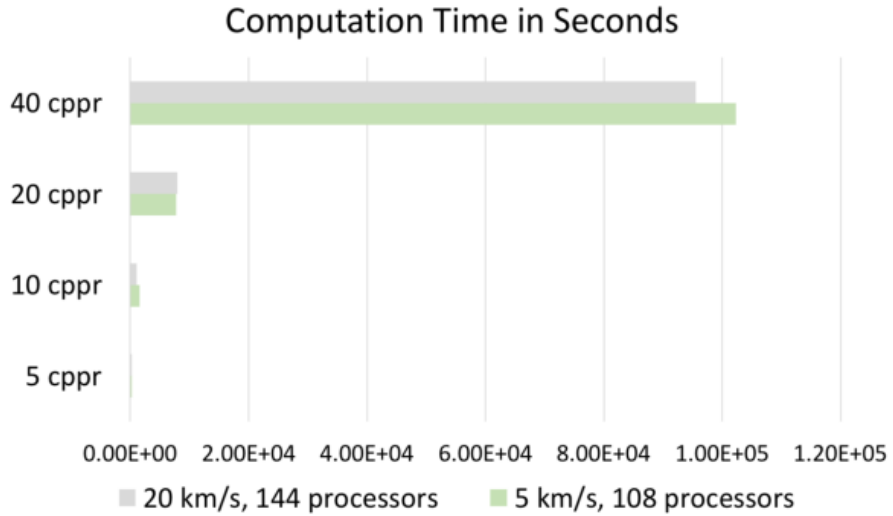

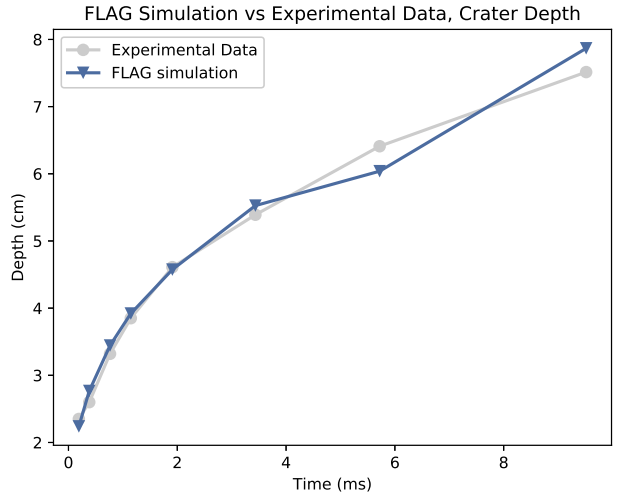

(Left) Computation times from FLAG mesh resolution study.† (Right) Crater depths from FLAG validation problem.†

Caldwell, W. K., A. Hunter, C. S. Plesko, and S. Wirkus. "Verification and Validation of the FLAG Hydrocode for Impact Cratering Simulations." *Journal of Verification, Validation and Uncertainty Quantification* 3(3):031004 (2019).

Asteroid 16 Psyche

- Largest M-type asteroid in Main Asteroid Belt
- Upcoming NASA mission Psyche: Journey to a Metal World
- Bulk density estimates: $1.4 \pm 0.3 - 4.5 \pm 1.4$ g/cm^3, some as high as 7.6 g/cm^3
- Believed to be differentiated planet core
- Two large impact structures in Southern hemisphere
  - 53 ± 15 km and 67 ± 15 km diameter
  - 6.4 ± 0.64 km depth
  - Crater formation dominated by strength rather than gravity

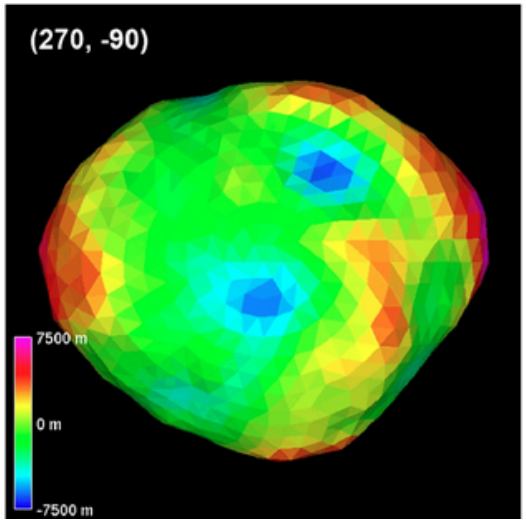

Image of Psyche with craters in blue. Image from Shepard et al., "Radar observations and shape model of asteroid 16 Psyche," *Icarus* (2017).

Larger Crater: 2D Axisymmetric Simulation Setup

- Resolution $\sim$ 15 cells per projectile radius (cppr)
- $\sim$ 2.3 million zones
- 180 processors
- Materials: Fe, Ni, SiO_2, Monel
- Psyche: semicircle, radius 125 km
- Impactor: semicircle, radius 5 km
- Void: (500 km $\times$ 500 km square)$\setminus$ (Psyche$\bigcup$ Impactor)

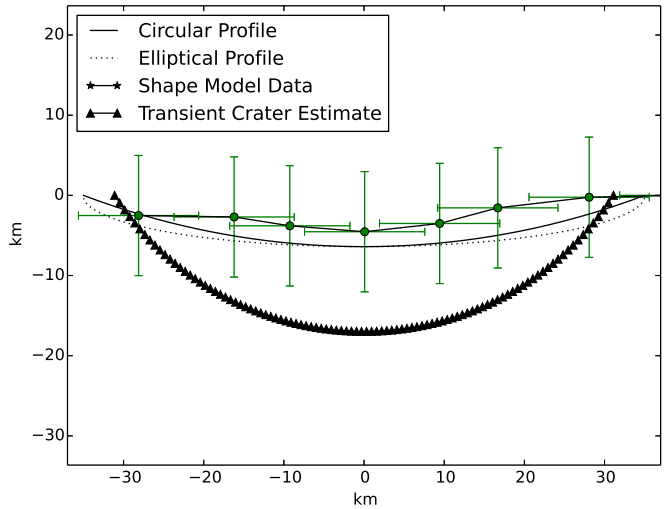

Theoretical crater profiles and shape model data for comparison. Image from Caldwell, “Differential Equation Models for Understanding Phenomena beyond Experimental Capabilities,” Arizona State University (2019).

Larger Crater: 2D Psyche Materials & Initialization

Material	ρ_0 $\left(\text{kg/m}^3\right)$	τ_Y (GPa)	G_0 (GPa)	Material Model	EOS
Fe	7795	0.05–0.275	87.2	PTW	SESAME
Monel	8810	0.838	68.8	SG	MG
Ni	8900 kg/m	0.14	85.5	SG	MG

(Left) 2D axisymmetric simulation at time 0 and (Right) zoomed to show detail.

Asteroid Obliteration

$$Q_D^* = Q_s + \frac{Q_B}{e^*}$$

$$Q_s \propto \frac{1}{\bar{R}}$$

$$Q_B = Q_G - Q_2 - Q_\omega; Q_B = F'' G\rho\bar{R}^2 \text{ (corrected)}$$

$$Q_G = FG\rho\bar{R}^2; Q_G \propto \frac{GM}{\bar{R}}$$

$$Q_2 = \frac{2\pi\sqrt[3]{2}G\rho\bar{R}^2}{5}$$

Asphaug, E., E. V. Ryan, and M. T. Zuber. "Asteroid Interiors," *Asteroids III*, University of Arizona Press (2002).

Dobrovolskis, A. R. and D. G. Korycansky. "Internal gravity, self-energy, and disruption of comets and asteroid," *Icarus* 303: 234–250 (2018).

Larger Crater: 2D Solid Results

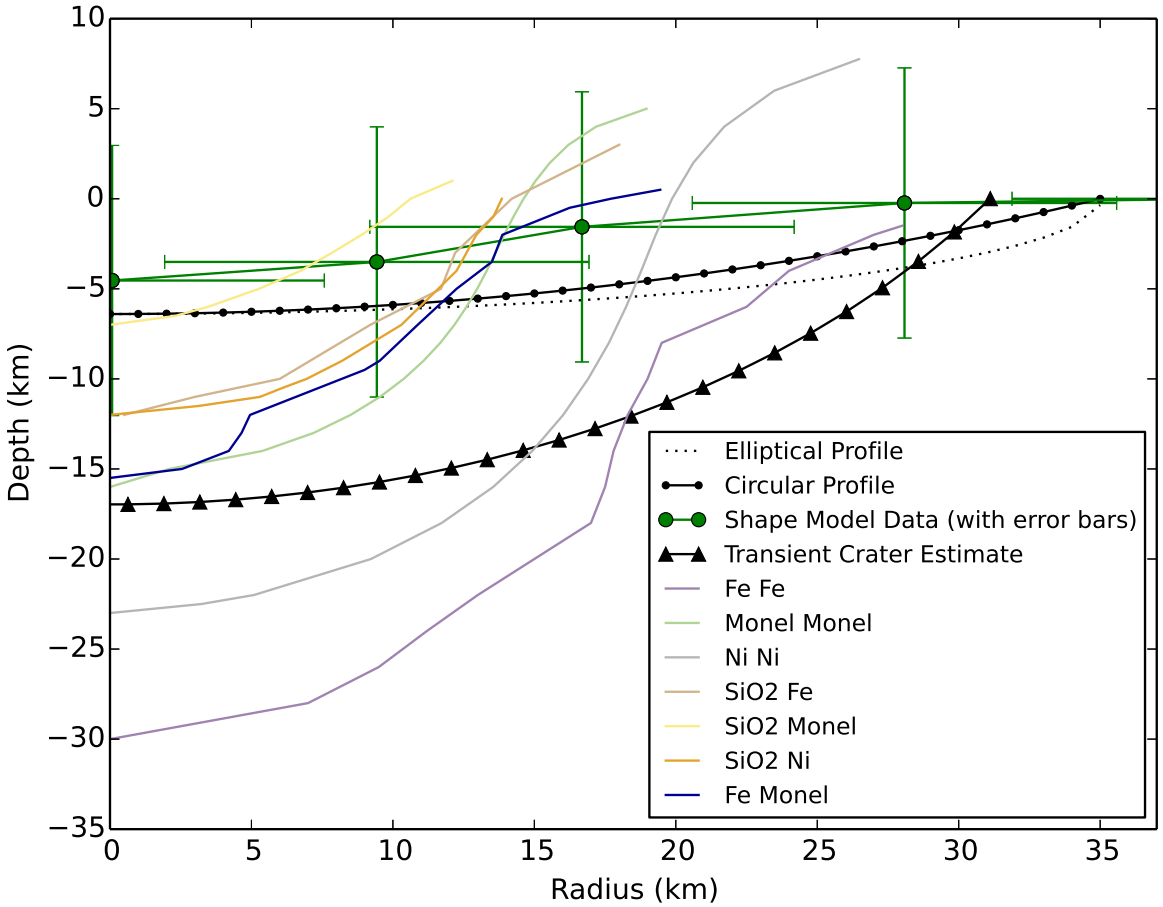

Crater profiles from simulations modeling Psyche as solid.

Larger Crater: 2D Target and Impactor Studies

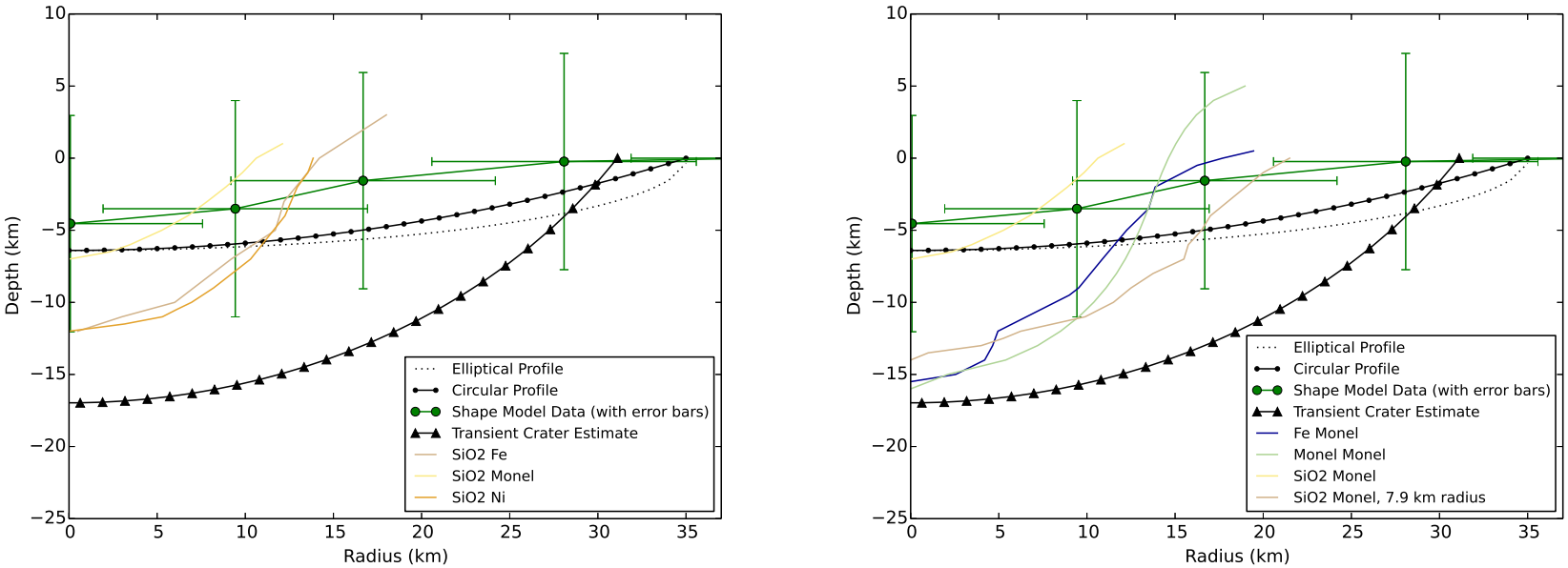

(Left) Target study with SiO_2 impactor. (Right) Impactor study with Monel target.

Crater dimensions appear to scale roughly with yield strength in the target study and density in the impactor study.

Larger Crater: 2D Porosity Study

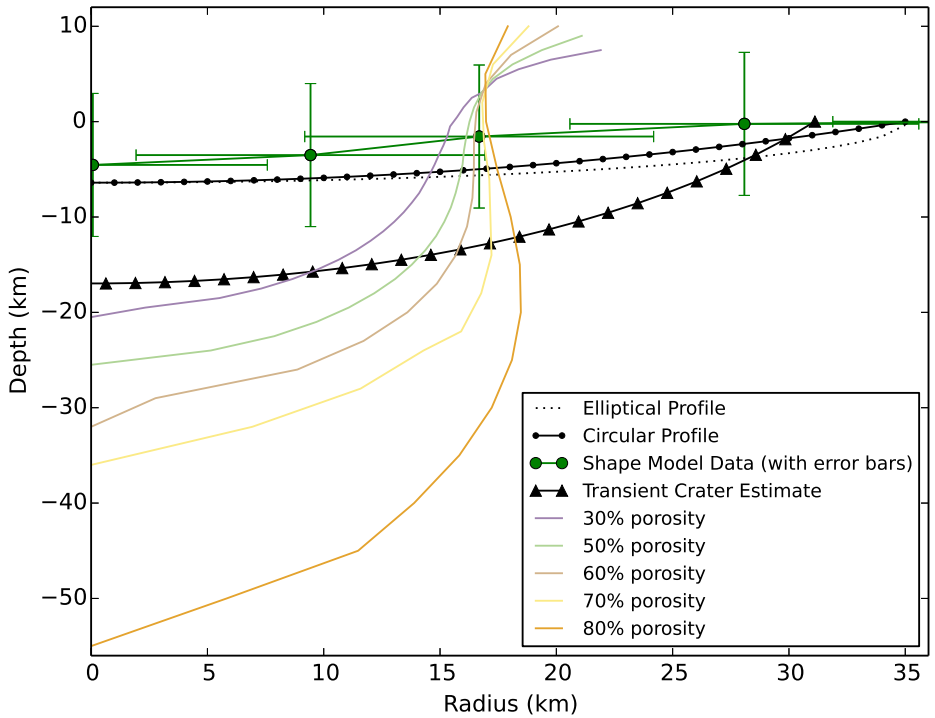

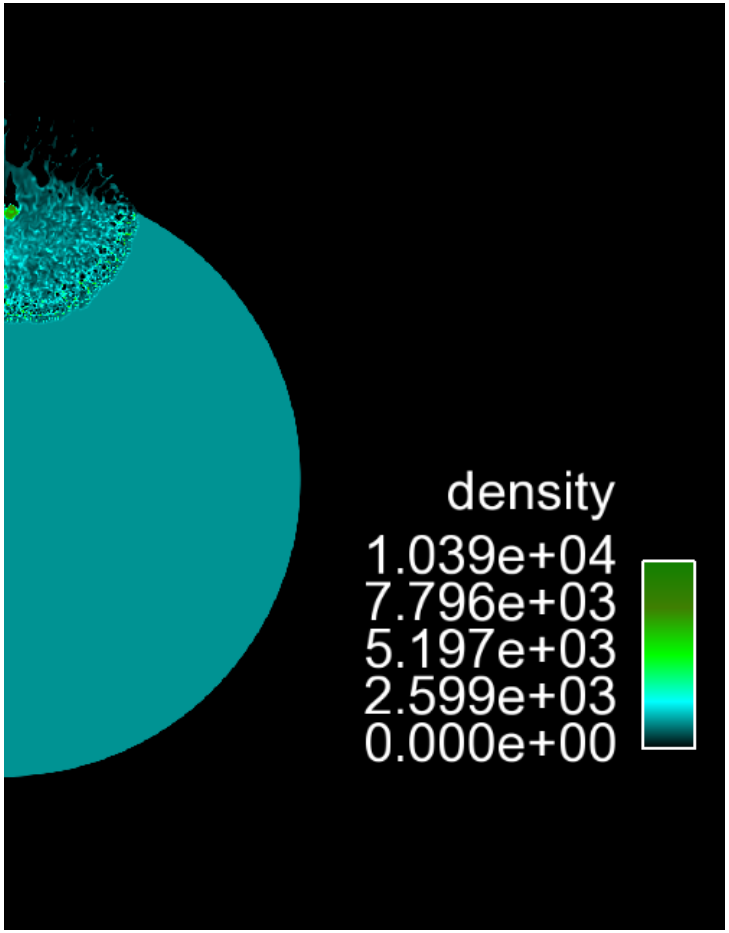

(Left) Crater profiles from 2D porosity study. (Right) Asteroid disruption from simulation with solid iron impacting 80% porous iron.

Larger Crater: 2D Results Summary

Simulation of solid SiO_2 impacting solid Monel, showing the overturned flap.

- Depth overestimation and diameter underestimation $\Longrightarrow$ oblique impact angle
- Porosity study $\Longrightarrow$ porosity likely around 30%–50%
- Impactor density and target yield stress key to crater formation
- 3D simulations are needed to vary impact angle.

Larger Crater: Psyche 3D Simulation Setup

- 3D Cartesian
- Psyche: Shape model, spherical cap of radius 110 km
- Impactor: Sphere, 5 km radius
- Void: Void Box $\setminus$ (Psyche & Impactor), 500 km x 500 km
- Zone size: 1000 m – 10000 m (5 cppr – 0.5 cppr)
- Zones: $\sim$ 33.4 million
- Proccesors: 1080

Video of Psyche simulation at initialization. Video credit: John Patchett; Shape model: Shepard et al., “Radar observations and shape model of asteroid 16 Psyche,” *Icarus* (2017).

Larger Crater: 3D Results

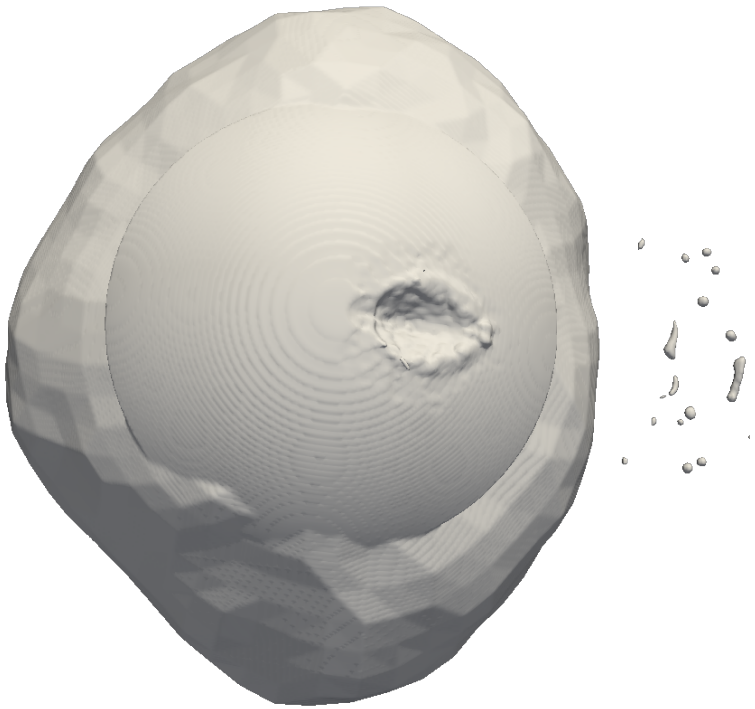

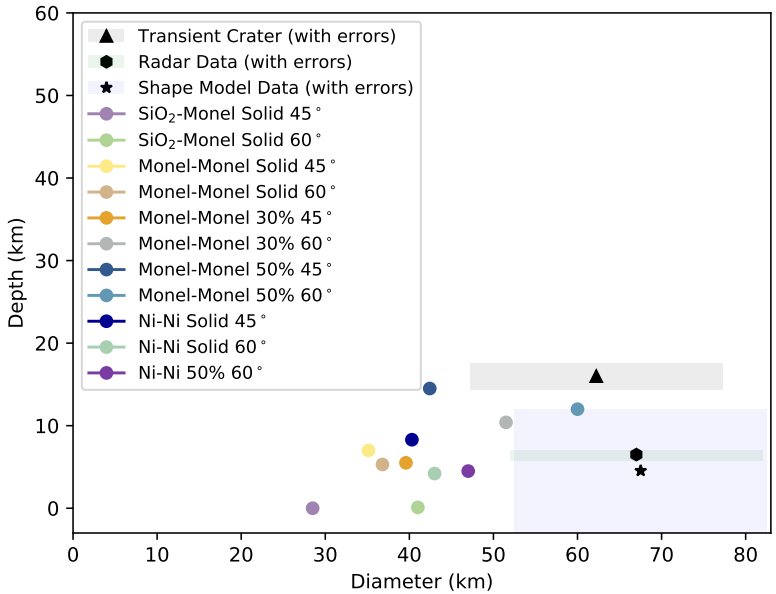

(Left) Crater formation from solid Monel impacting 50% porous Monel 60° from vertical, about 40 seconds after impact.
(Right) Crater aspect ratios from 3D simulations, with shaded uncertainties.

Larger Crater: 3D Profiles

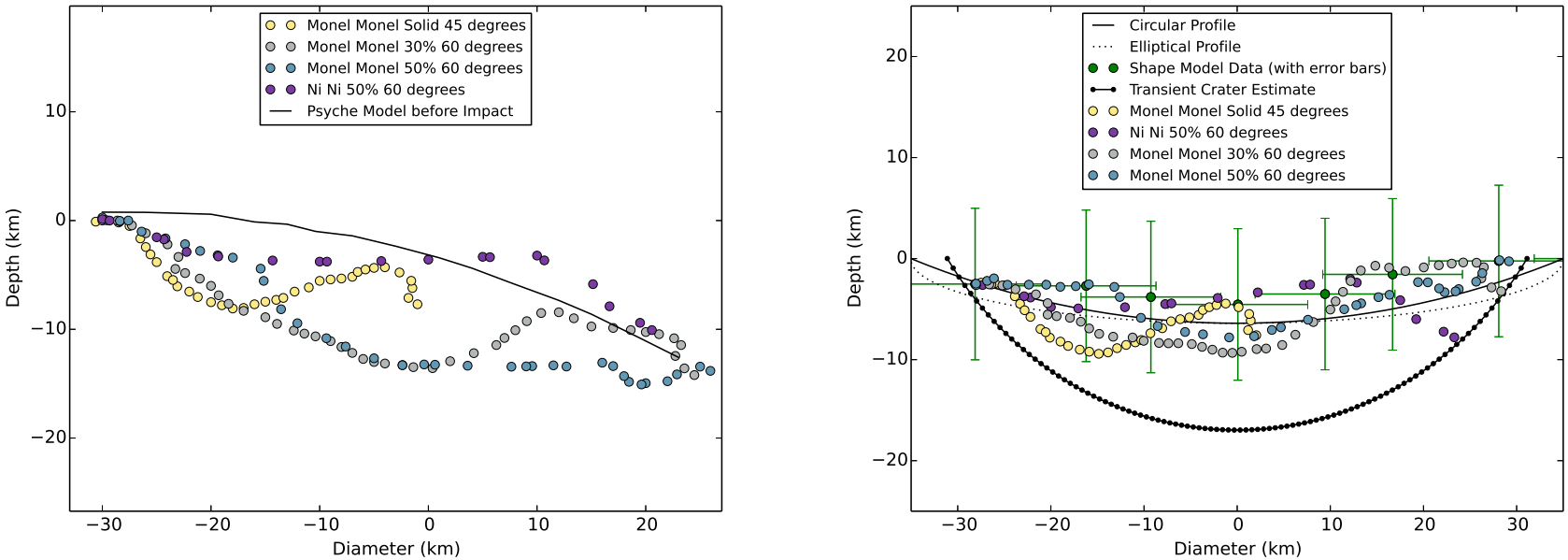

(Left) Crater profiles from 3D simulations with closest matches to diameter and depth, plotted alongside the pre-impact simulation surface. (Right) Simulation profiles rotated to align with shape model for ease of comparison.

Larger Crater: 3D Results

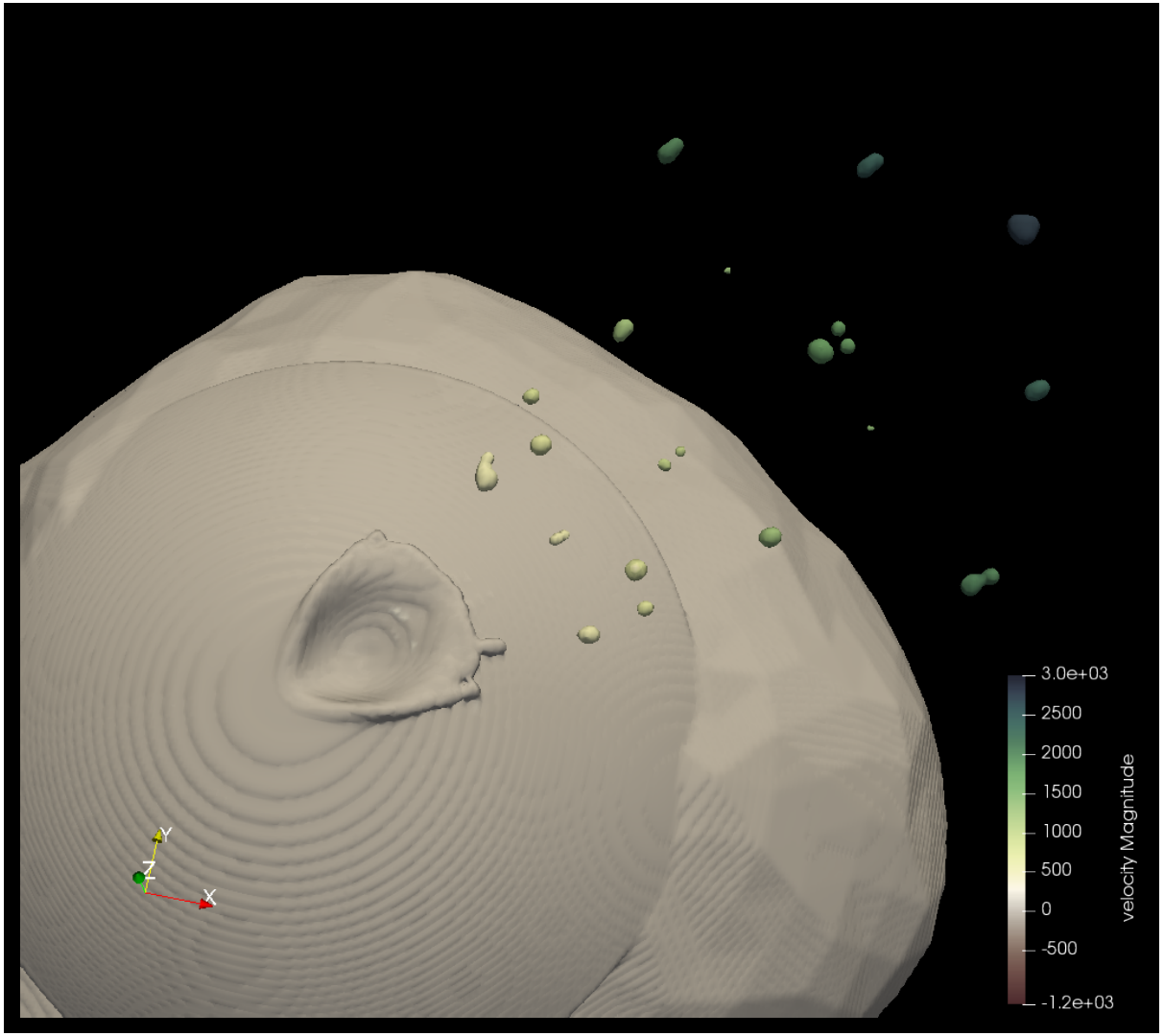

FLAG simulation of Monel-Monel 45° impact about 92 seconds after impact, colored by velocity.

Larger Crater: 3D Simulation Video

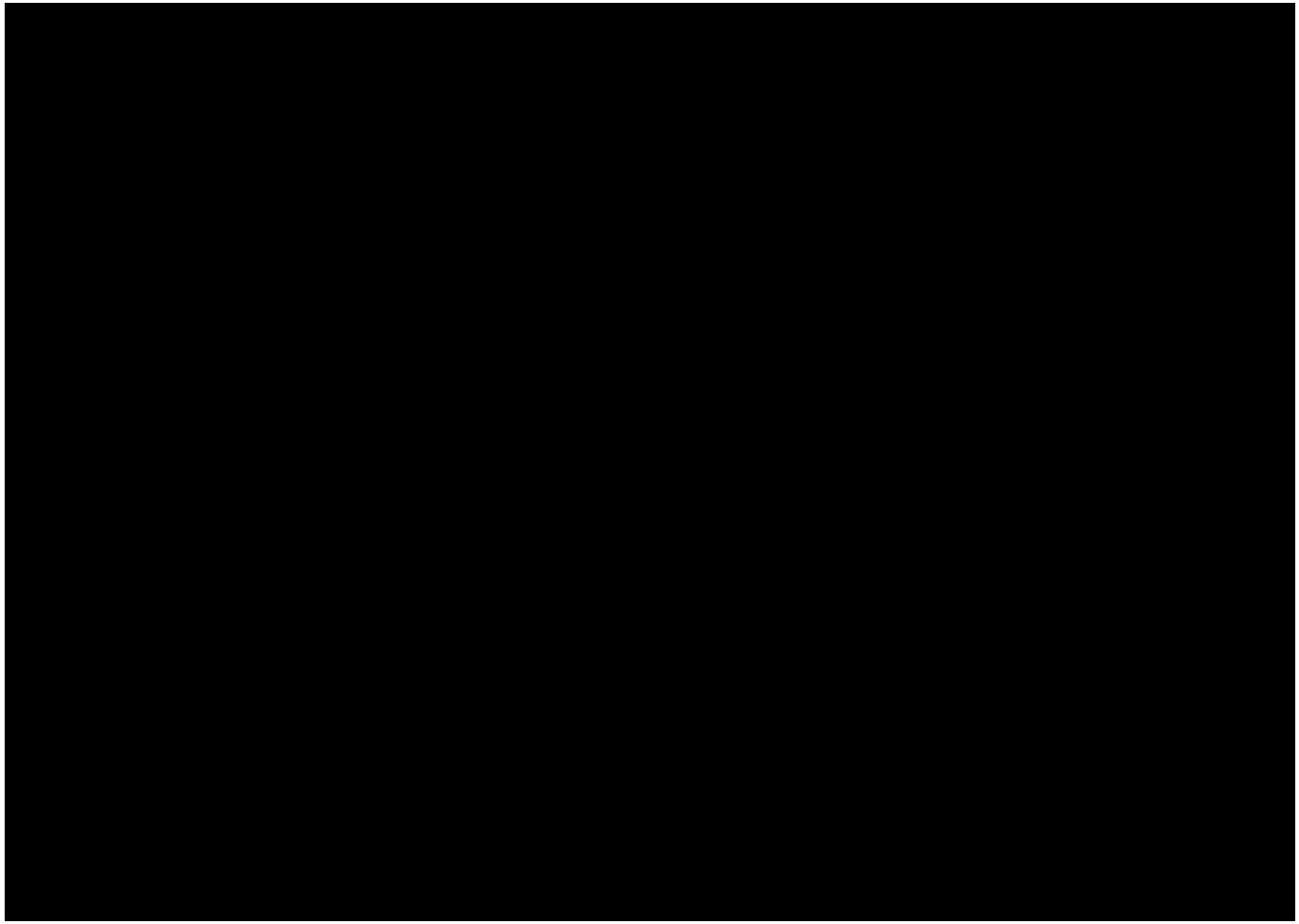

Simulation video of solid Monel impacting 50% porous Monel 60° from vertical. Video credit: John Patchett; Shape model: Shepard et al., “Radar observations and shape model of asteroid 16 Psyche,” *Icarus* (2017).

3D Results Summary

- Impact angle likely oblique $> 45^\circ$
- Likely 30%–50% porous
- Best matches
  - Monel-Monel, 50% porosity, 60° from vertical
  - Monel-Monel, 30% porosity, 60° from vertical
  - Ni-Ni, 50% porosity, 60° from vertical
- Yield stress appeared to dominate in 2D, while this trend did not hold for 3D
- Many simulations considerably underestimated diameter $\Longrightarrow$ porosity may not be homogeneous
- 3D simulations provide more robust studies

Smaller Crater: Preliminary Results

- Resolution $\sim$ 11 cppr
- $\sim$ 2.3 million zones
- 180 processors
- Materials: Fe, Ni, SiO_2, Monel
- Psyche: semicircle, radius 125 km
- Impactor: semicircle, radius 3.75 km
- Void: (500 km 500 km square) $\setminus$ (Psyche $\bigcup$ Impactor)

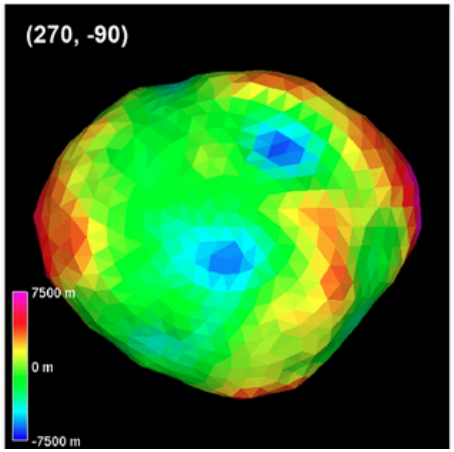

Image of Psyche with craters in blue. Image from Shepard et al., "Radar observations and shape model of asteroid 16 Psyche," *Icarus* (2017).

Smaller Crater: Preliminary Results

Solid targets: underestimated diameter

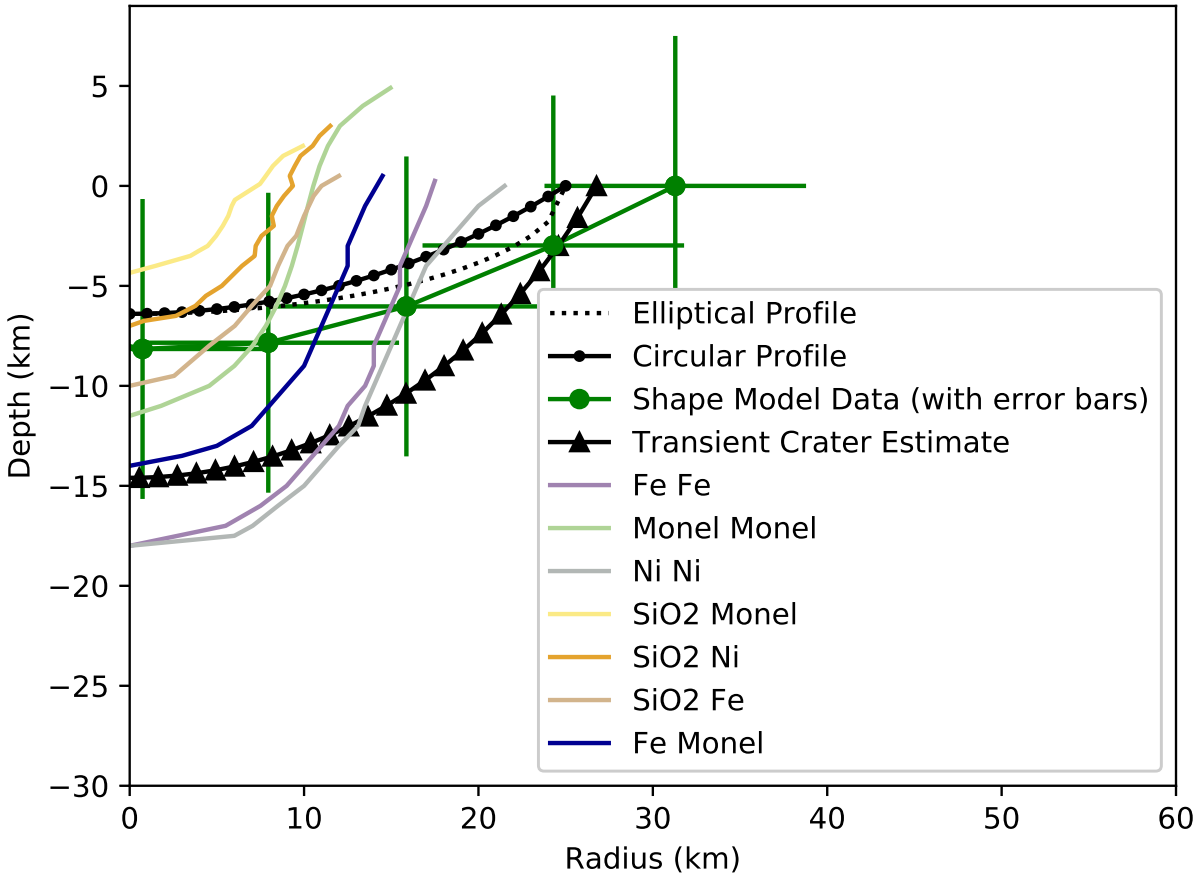

Crater profiles from 2D axisymmetric simulations testing solid impactors and solid targets.

Smaller Crater: Preliminary 3D Results

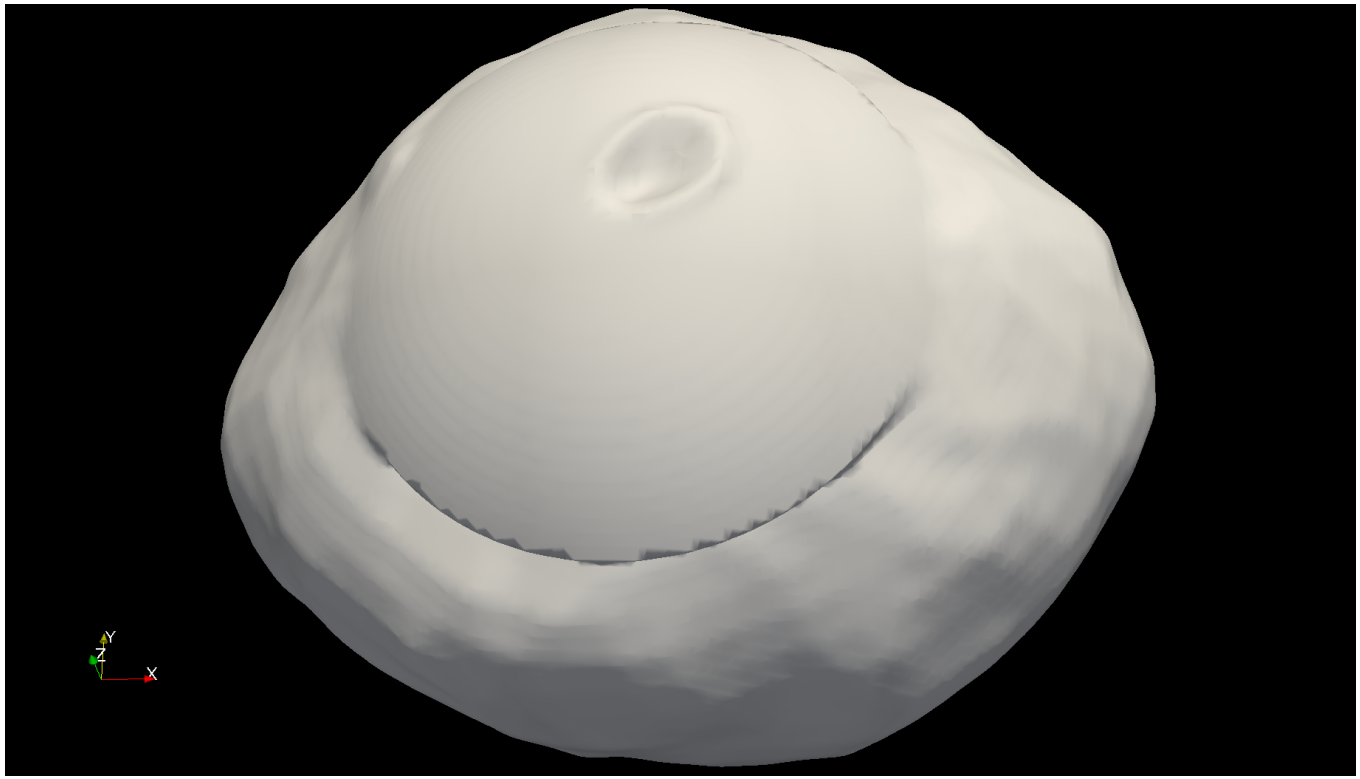

3D FLAG simulation of Ni-Ni 45° solid impact. The crater diameter was 38.18 km, and the crater depth was 5.5 km. This preliminary result is from a coarse run of resolution 2 cppr. The diameter is within the error bars for the shape model, and the depth is within the error bar if correcting for the underestimation expected from coarse resolutions in FLAG.

Smaller Crater: Preliminary Results

Non-homogeneous porosity

- Inner Radius 100 km
  Outer Radius 25 km

φ_{inner}	φ_{outer}	ρ_{bulk}
40%	70%	4335
40%	80%	4017
50%	60%	4088
50%	70%	3771
50%	80%	3454
60%	70%	3207
60%	80%	2890

- Inner Radius 110 km
  Outer Radius 15 km

φ_{inner}	φ_{outer}	ρ_{bulk}
50%	60%	4206
50%	70%	4007
50%	80%	3808
60%	70%	3325
60%	80%	3126

- Inner Radius 120 km
  Outer Radius 5 km

φ_{inner}	φ_{outer}	ρ_{bulk}
50%	60%	4336
50%	70%	4267
50%	80%	4198
60%	70%	3455
60%	80%	3386

Densities are listed in kg/m^3.

Smaller Crater: Preliminary Results

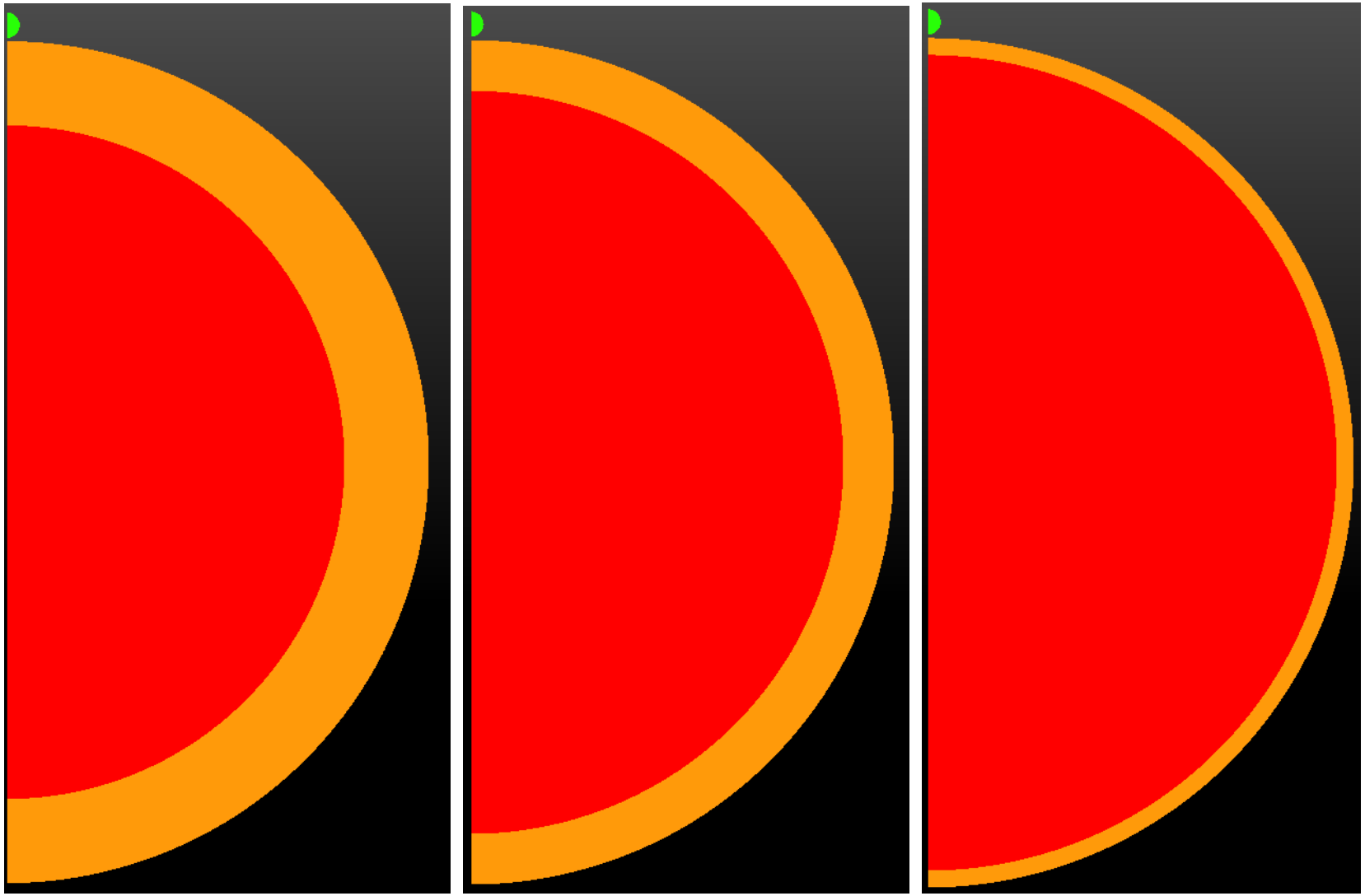

Simulation setups with (Left) inner radius 100 km and outer radius 25 km, (Center) inner radius 110 km and outer radius 15 km, and (Right) inner radius 120 km and outer radius 5 km.

Smaller Crater: Preliminary Results

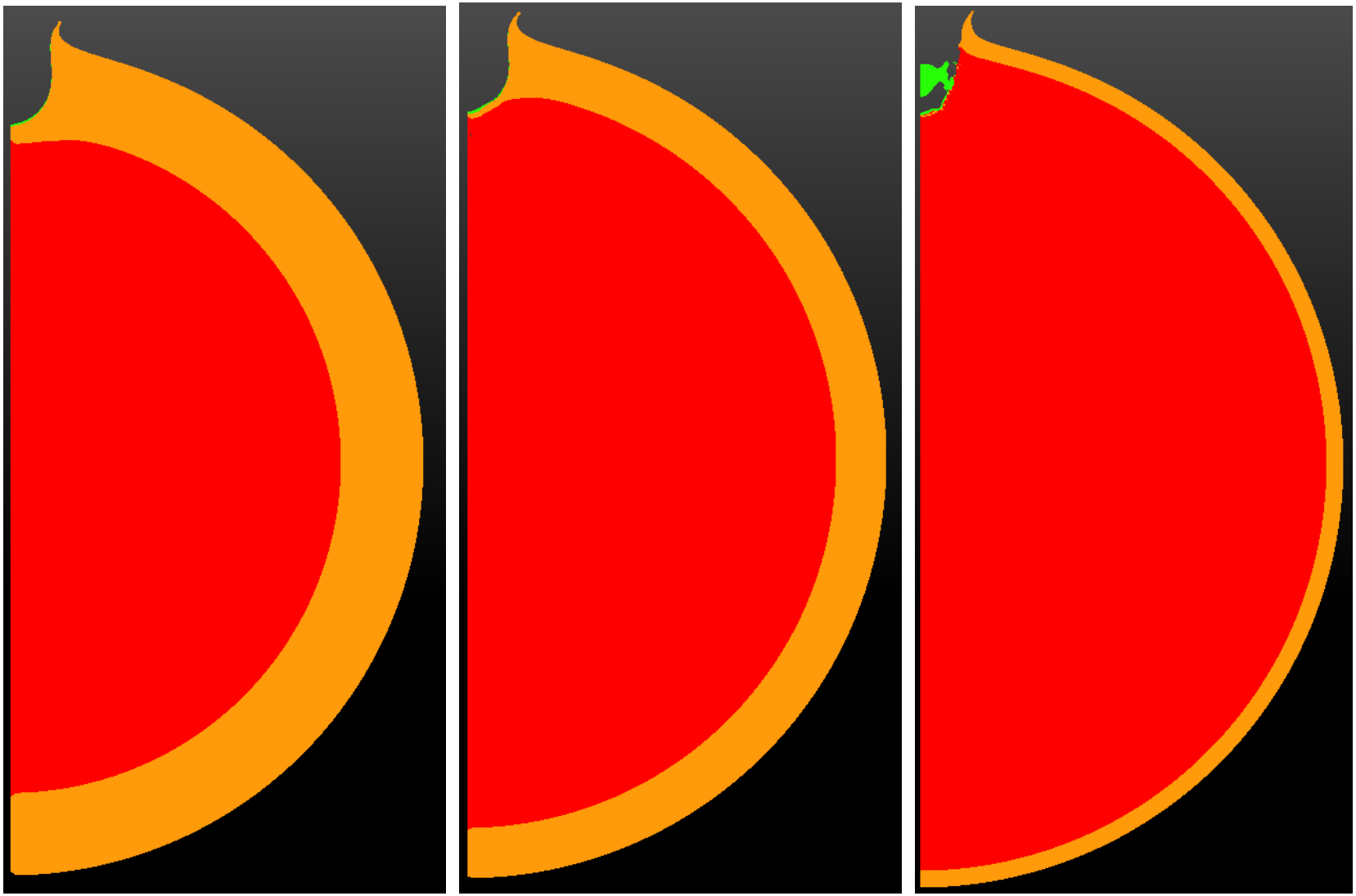

Simulations with inner $\varphi = 50\%$ and (Left) outer $\varphi = 60\%$ $\sim$270 s after impact, (Center) outer $\varphi = 60\%$ $\sim$255 s after impact, and (Right) outer $\phi = 70\%$ $\sim$25.5 s after impact.

Smaller Crater: Preliminary Results

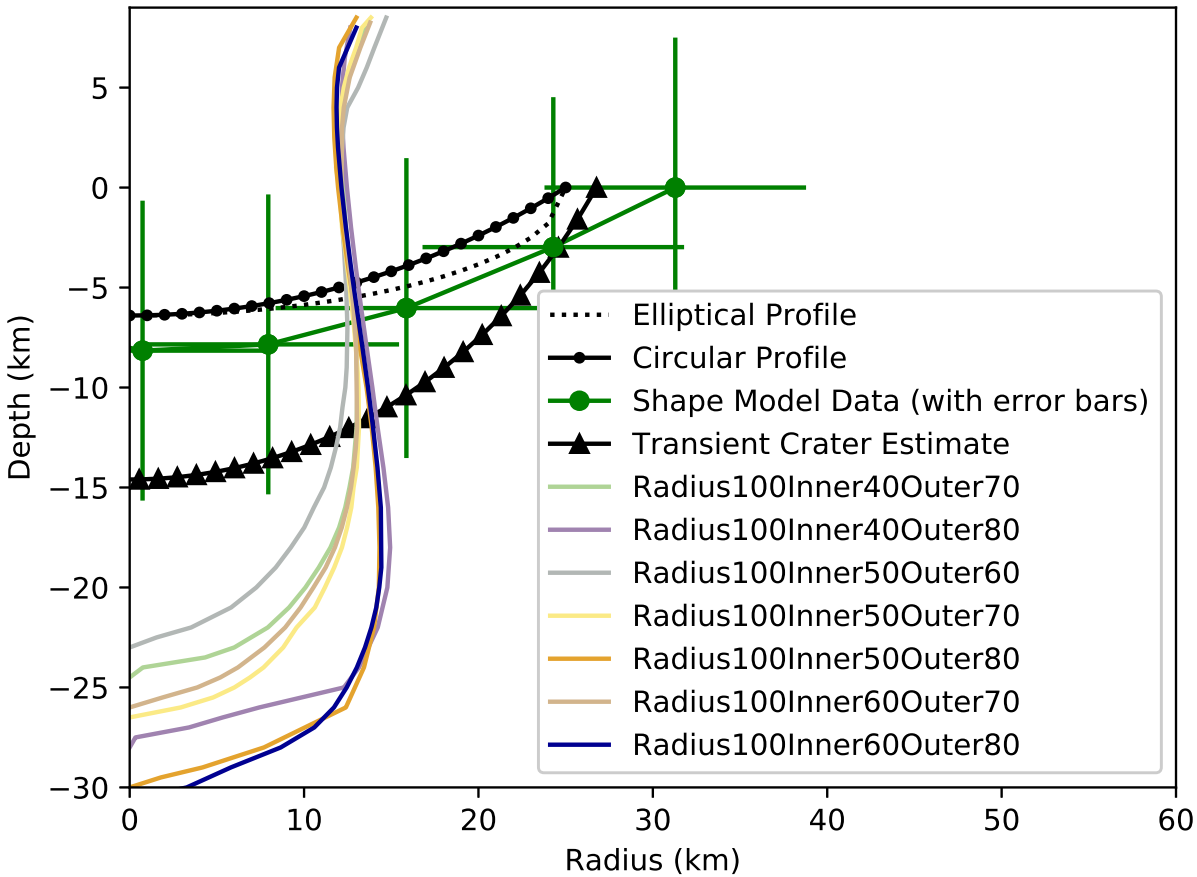

Crater profiles from simulations with an inner radius of 100 km and an outer radius of 25 km, varying the densities and porosities in each part.

Smaller Crater: Preliminary Results

Lessons Learned

- Solid: Mostly reasonable depths, underestimated diameters
- Non-homogeneous porosity: large discrepancies in both depths and diameters
- Larger crater results indicate porosity may not be homogeneous throughout

Smaller Crater: Preliminary Results

Rubble pile: hexagonal packing
Circle radius: 12.5 km
Macroporosity: 7.7%

Microporosity	Bulk Density
0 %	8129.643 kg/m^3
30 %	5690.750 kg/m^3
40 %	4877.786 kg/m^3
50 %	4064.822 kg/m^3

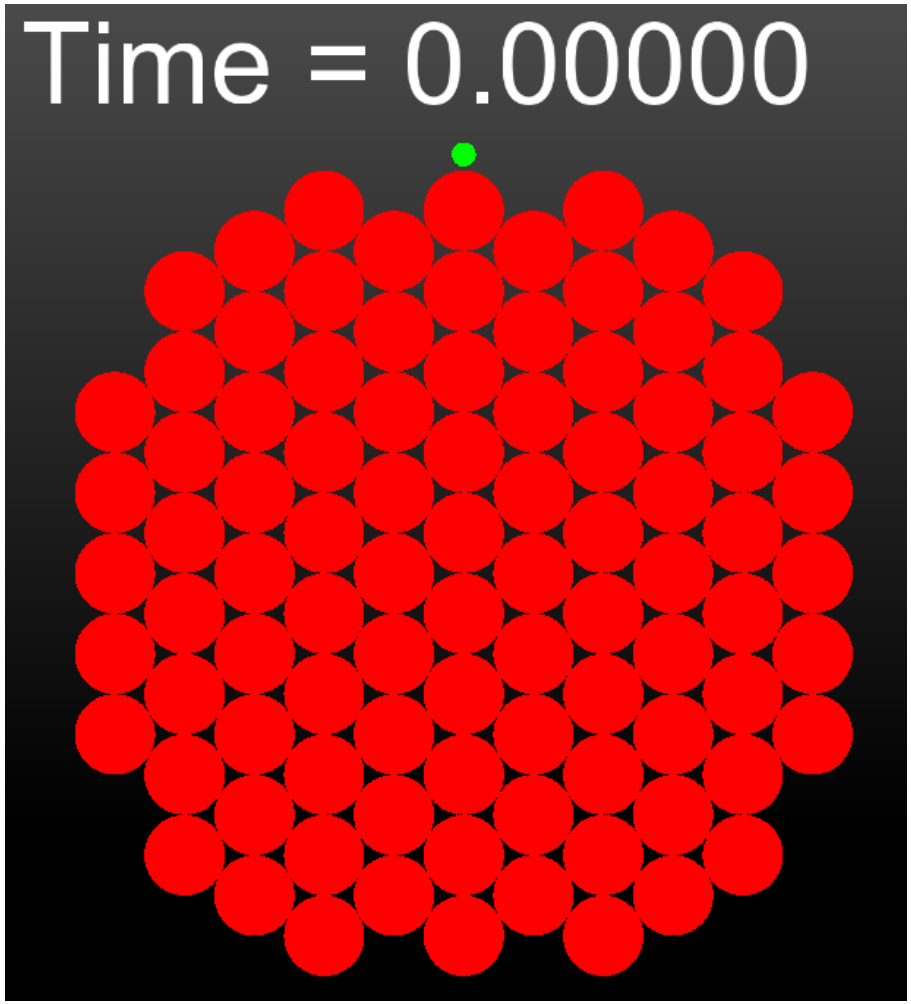

Smaller Crater: Preliminary Results

Rubble pile: square packing
Circle radius: 12.5 km
Macroporosity: 17.4%

Microporosity	Bulk Density
0 %	7279.883 kg/m^3
30 %	5095.918 kg/m^3
40 %	4367.930 kg/m^3
50 %	3639.942 kg/m^3

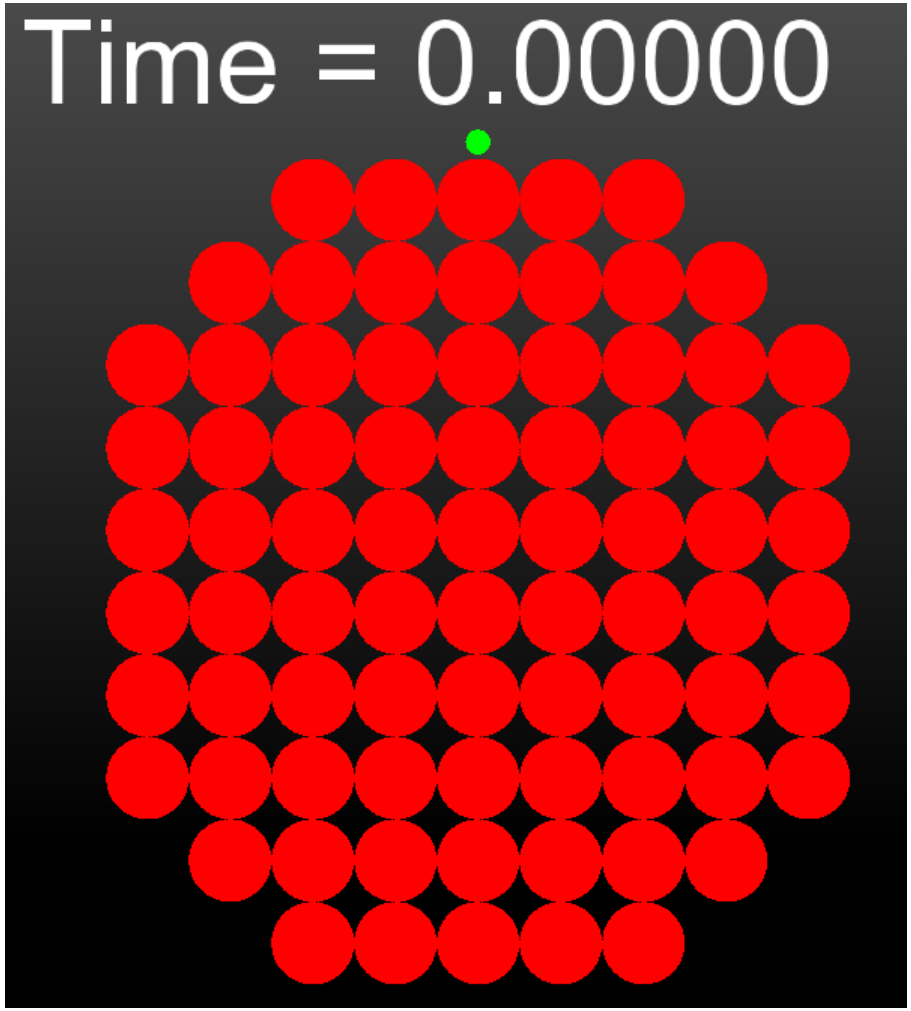

Smaller Crater: Preliminary Results

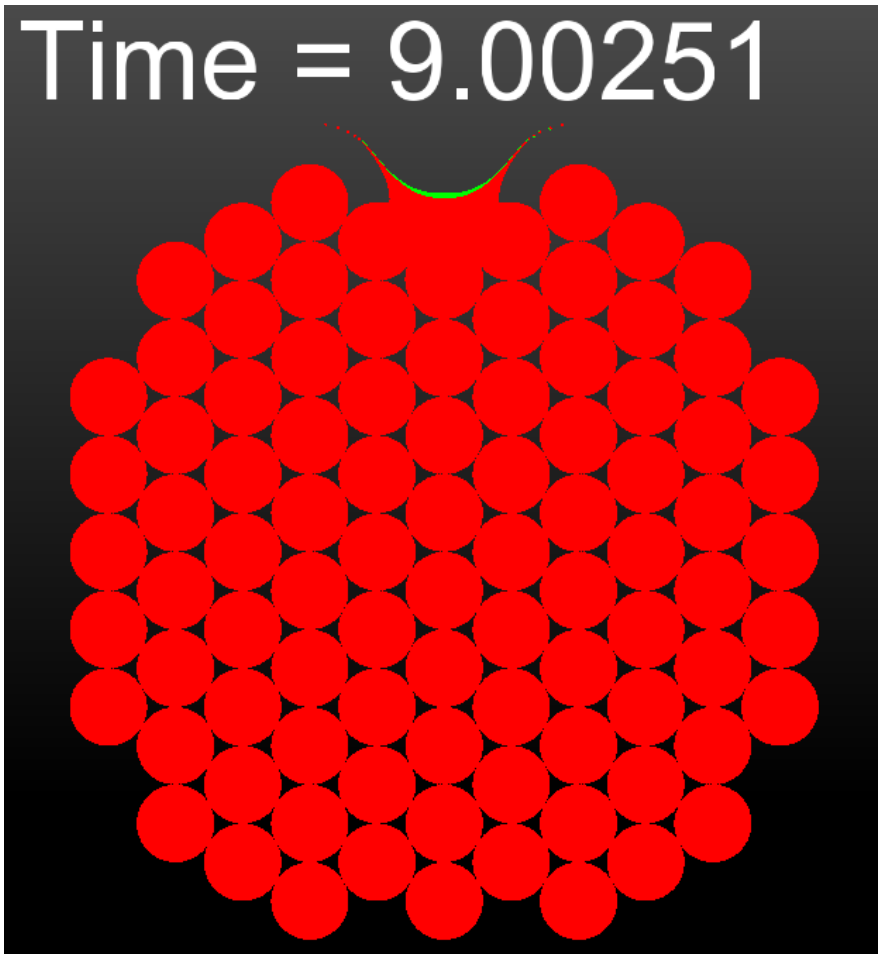

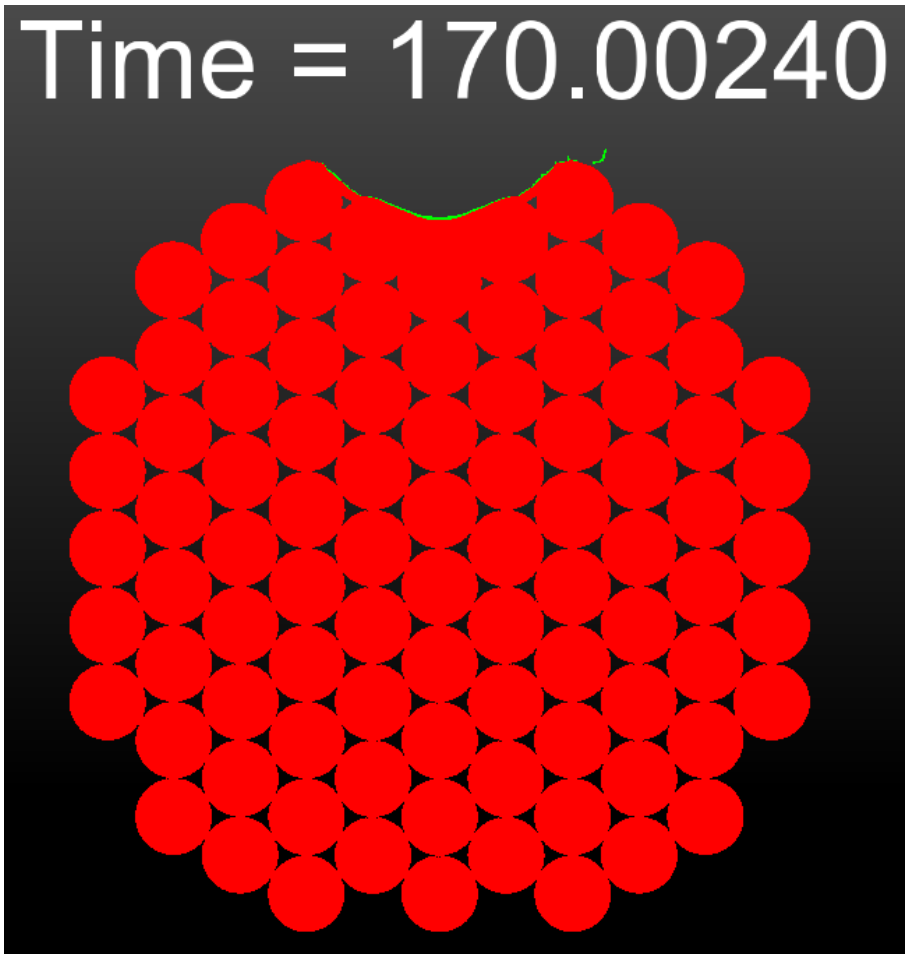

Smaller Crater: Preliminary Results

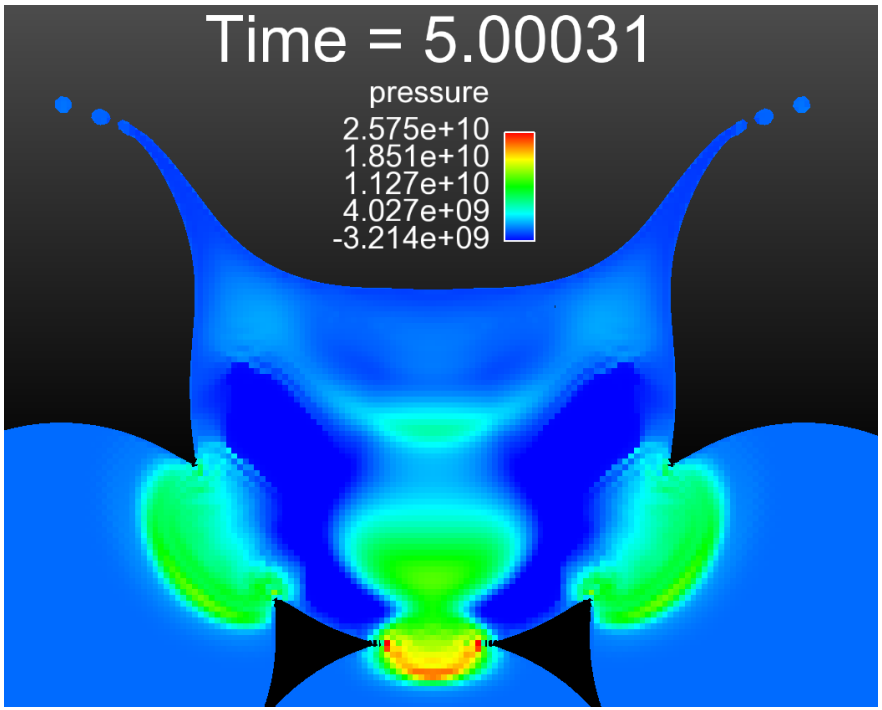

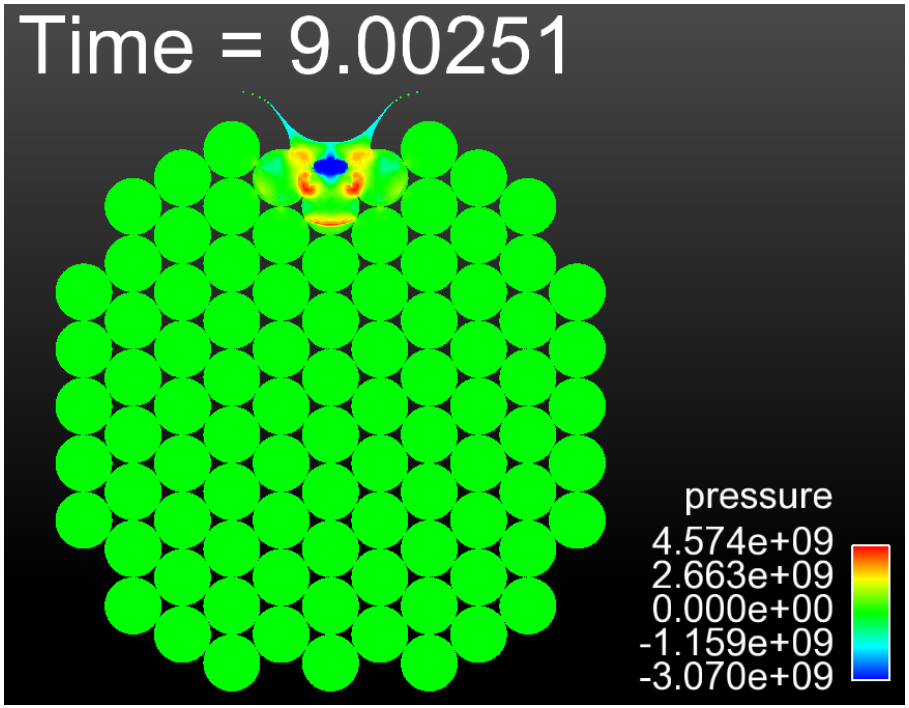

Smaller Crater: Preliminary Results

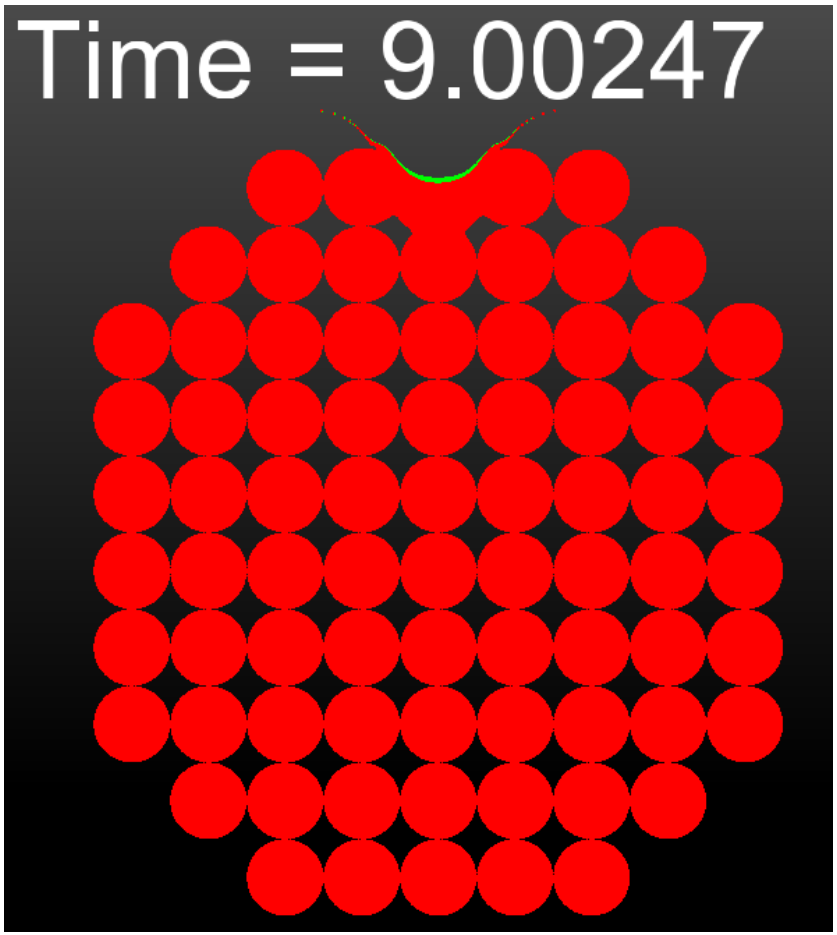

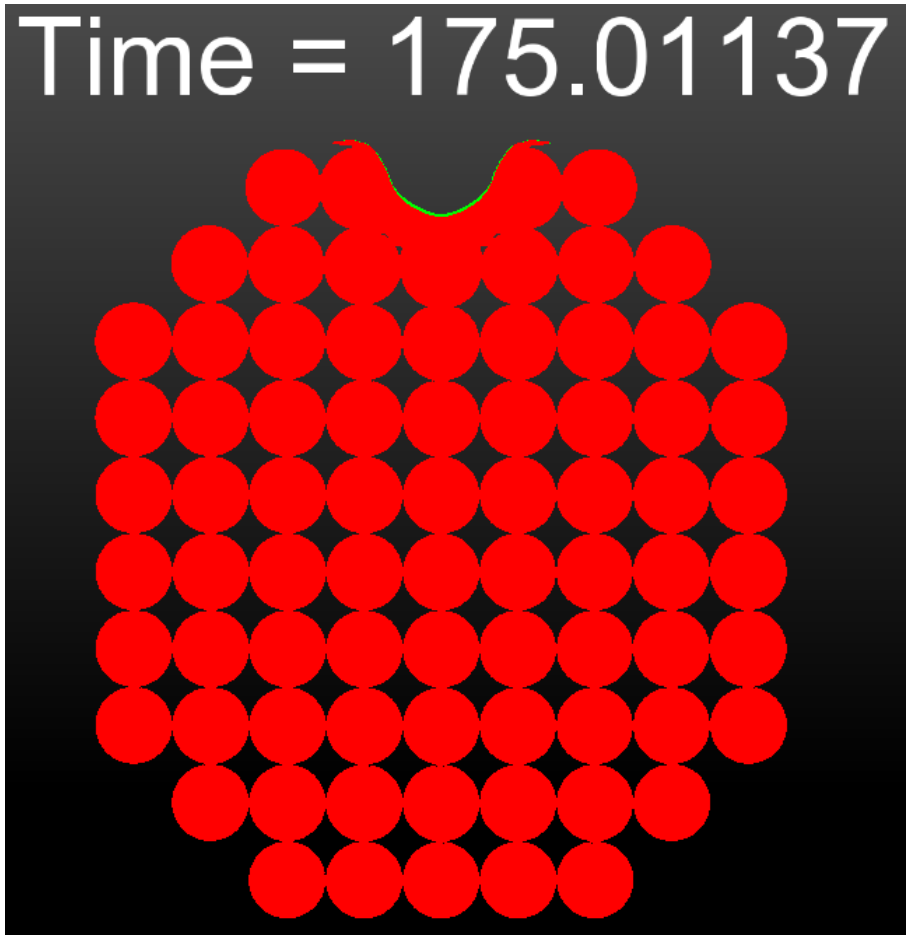

Smaller Crater: Preliminary Results

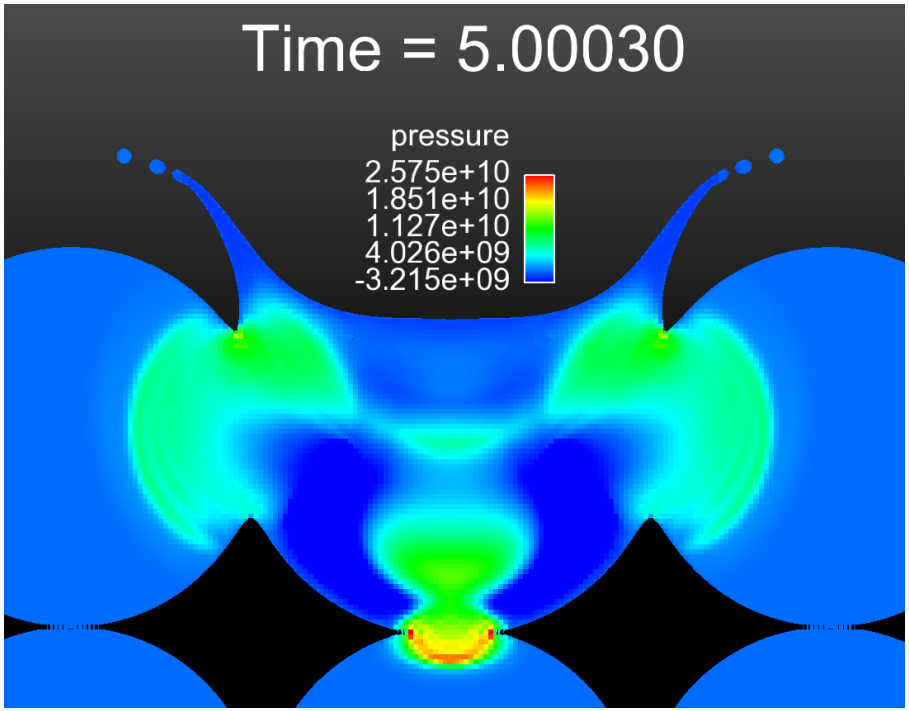

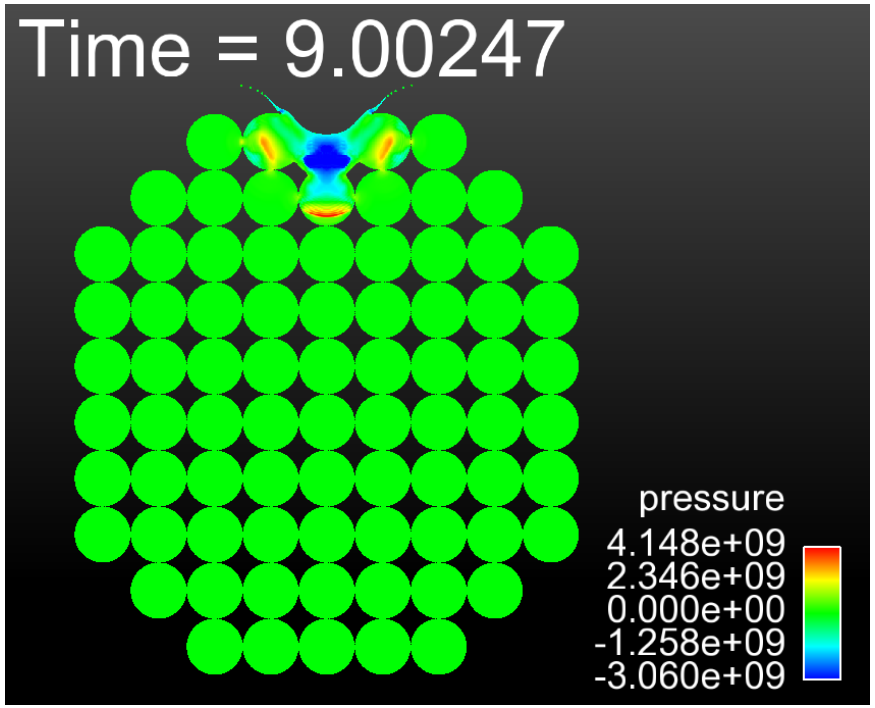

Smaller Crater: Preliminary Results

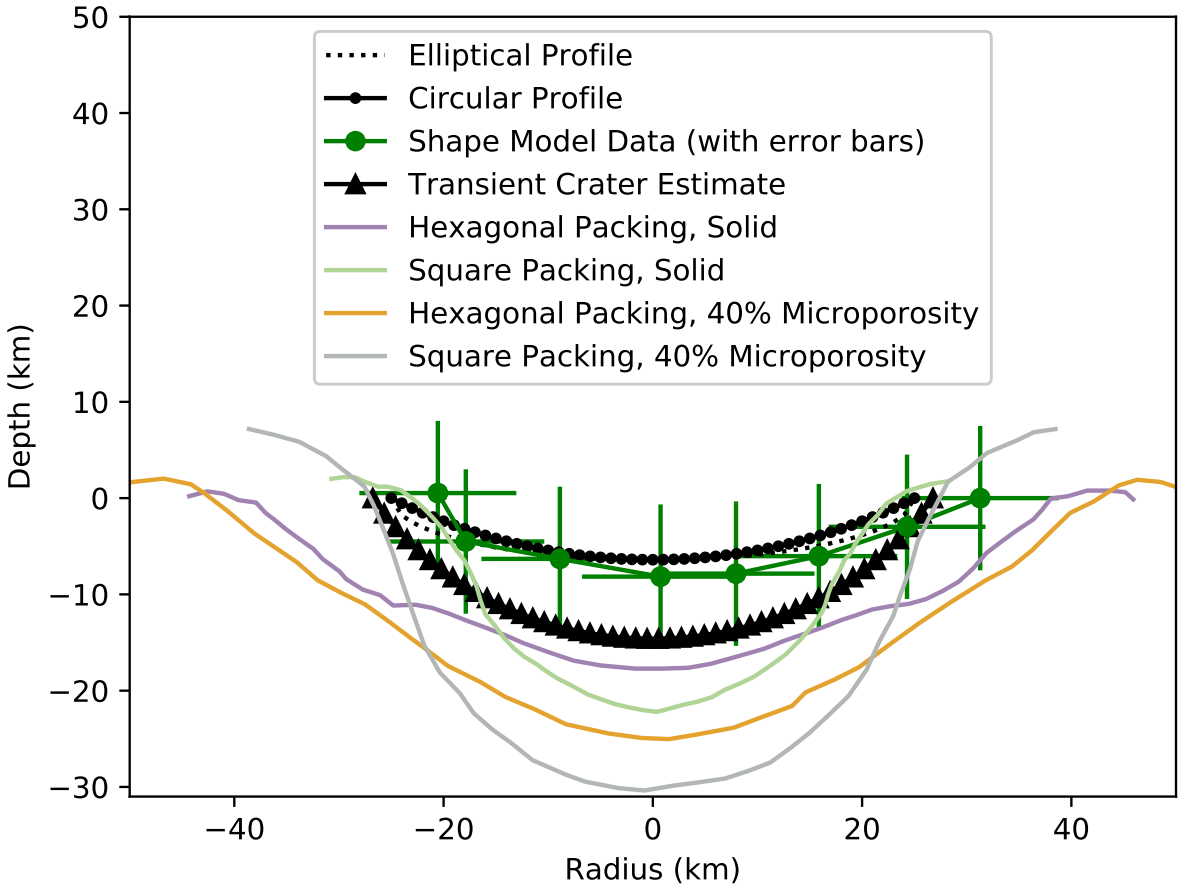

Crater profiles from 2D Cartesian simulations of rubble piles with microporosity.

Forthcoming Work

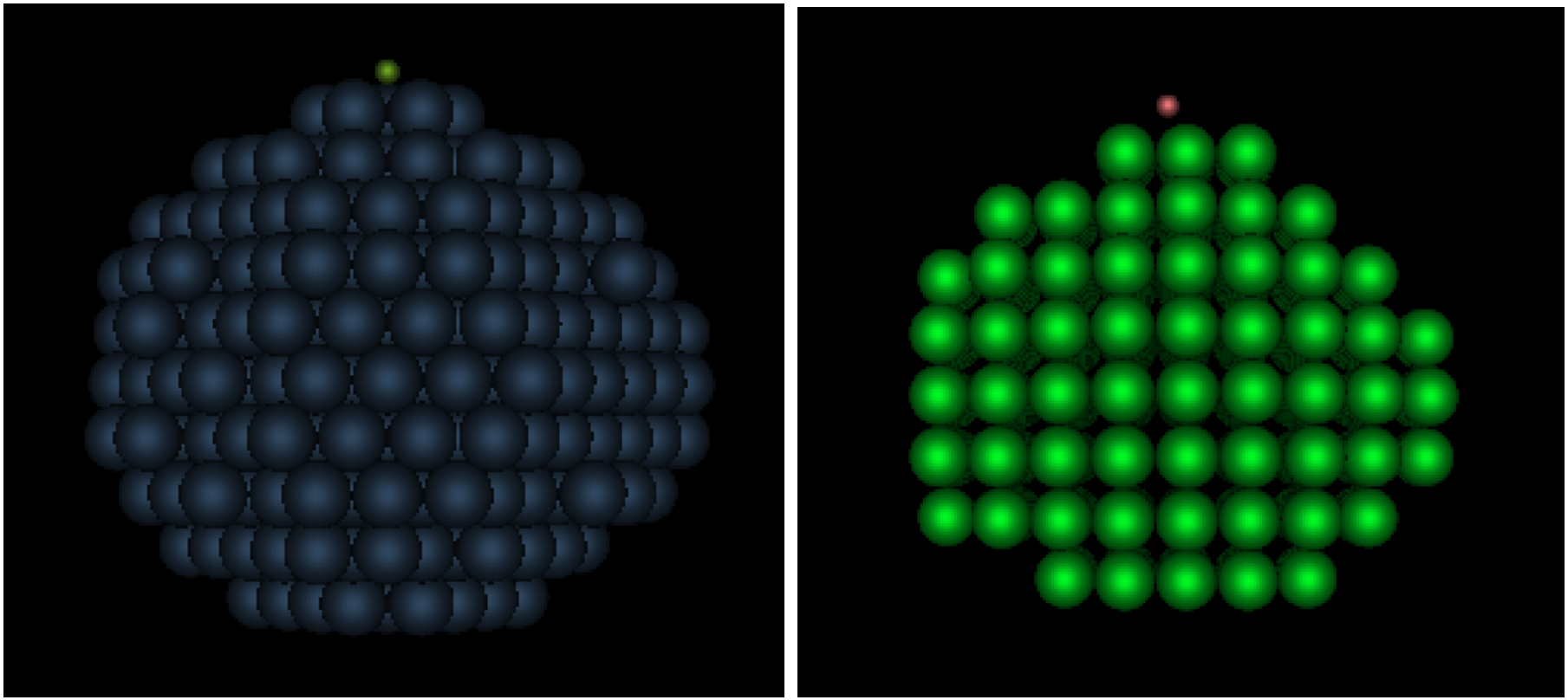

(Left) 3D simulation setup with close hexagonal packing. (Right) 3D simulation setup with square packing.

Forthcoming Work

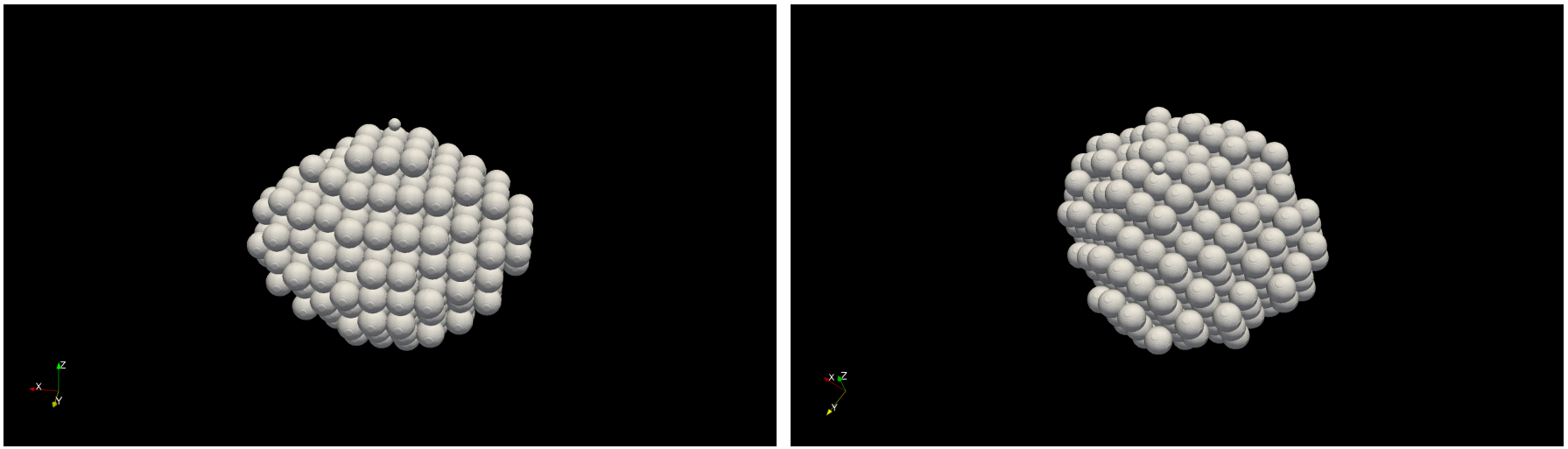

Initialization of simulation of formation of Psyche's largest crater, modeled as a rubble pile of 12.5 km spheres in a square packing.

Forthcoming Work

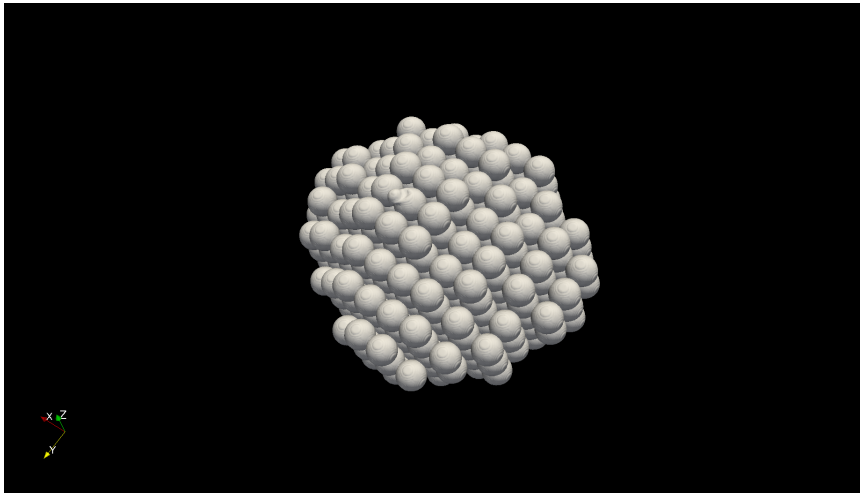
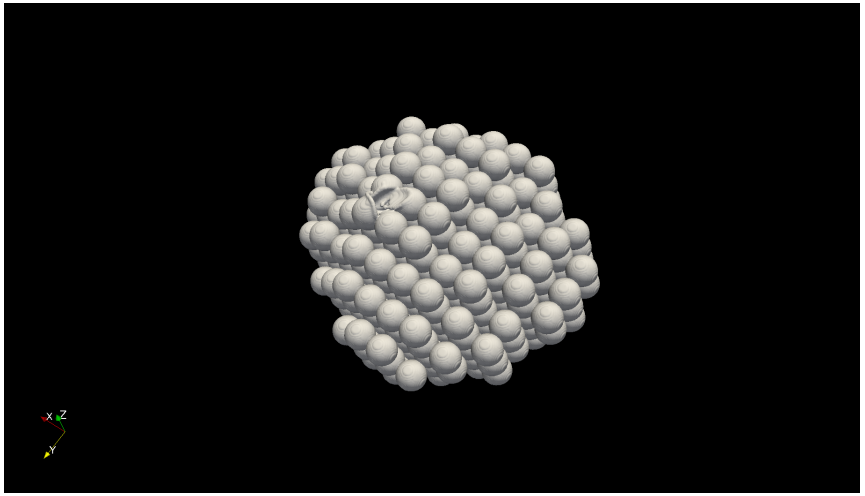

Crater formation from simulation of 3D square-packed rubble pile (Left) 5 s (Right) 10 s after impact.

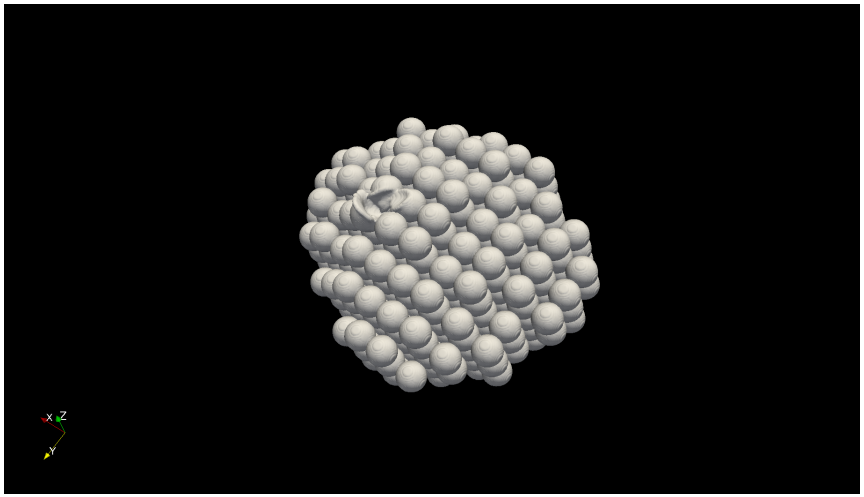
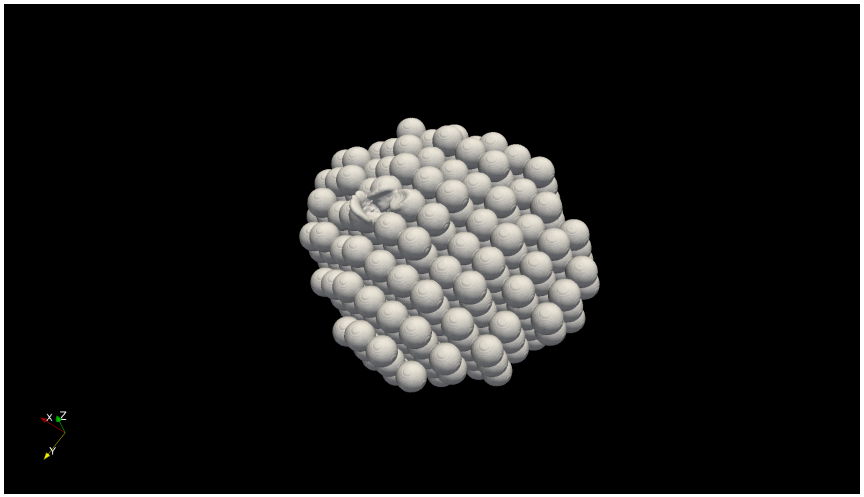

Largest crater formation from simulation of 3D square-packed rubble pile (Left) 15 s (Right) 381 s after impact.

Forthcoming Work

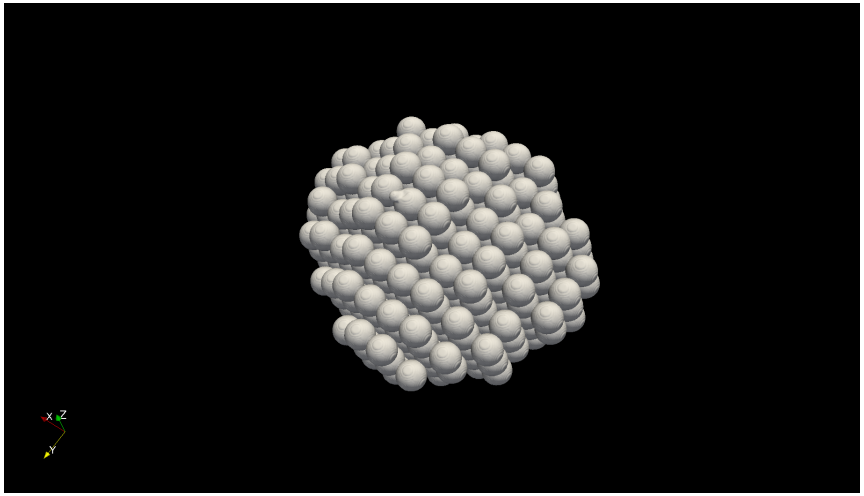
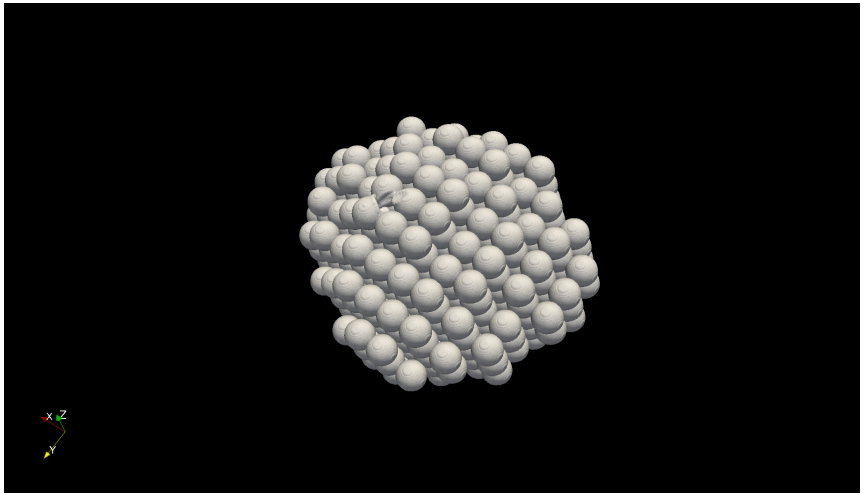

Crater formation from simulation of 3D square-packed rubble pile (Left) 5 s (Right) 10 s after impact.

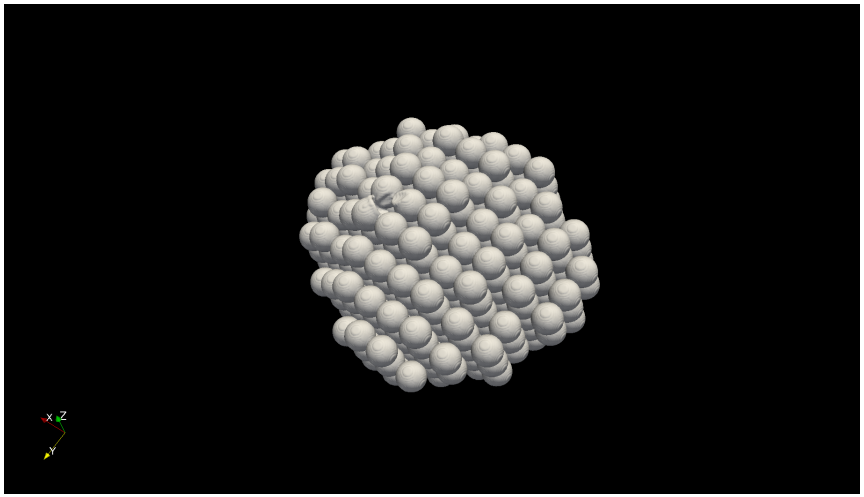
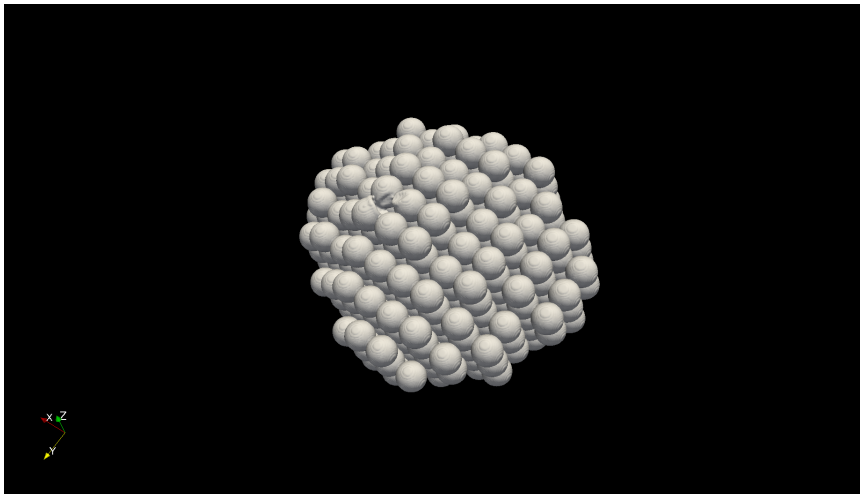

Smaller crater formation from simulation of 3D square-packed rubble pile (Left) 15 s (Right) 381 s after impact.

References

Burton, D. “Consistent Finite-Volume Discretization of Hydrodynamic Conservation Laws for Unstructured Grids,” Tech. Rep. UCRL-JC-118306, Lawrence Livermore National Laboratory, Livermore, CA (1994).

Caldwell, W. K., A. Hunter, C. S. Plesko, S. Wirkus. “Verification and Validation of the FLAG Hydrocode for Impact Cratering Simulations,” *Journal of Verification, Validation and Uncertainty Quantification* 3(3):031004 (2019).

Farinella, P. and D. R. Davis. “Collision Rates and Impact Velocities in the Main Asteroid Belt,” *Icarus* 97(1):111–123 (1992).

Holsapple, K. A. “Impact and Explosion Effects,” http://keith.aa.washington.edu/craterdata/scaling/index.htm (2018).

Lupishko, D. “On the Bulk Density of the M-type Asteroid 16 Psyche,” *Solar System Research* 40(3):214–218 (2006).

Oh, D. Y. et al. “Psyche: Journal to a Metal World,” 52nd AIAA/SAE/ASEE Joint Propulsion Conference, p. 4541 (2016).

Pierazzo, E. et al. “Validation of numerical codes for impact and explosion cratering: Impacts on strengthless and metal targets,” *Meteoritics & Planetary Science* 43(12):1917–1938 (2008).

Shepard, M. K. et al. “Radar observations and shape model of asteroid 16 Psyche,” *Icarus* 281:388–403 (2017).

Acknowledgments

This work was supported in part by a completion fellowship from the Arizona State University Graduate College, a grant from the Center for Space and Earth Science for Research and Development in Space Science, the Advanced Simulation and Computing (ASC)–Integrated Codes program at Los Alamos National Laboratory (LANL), and the ASC–Threat Reduction program at LANL. Los Alamos National Laboratory, an affirmative action/equal opportunity employer, is operated by Triad National Security, LLC, for the National Nuclear Security Administration of the U.S. Department of Energy under contract 89233218NCA000001.

Conservation Laws and Hugoniot Equations

Conservation Laws

Momentum: $\rho \frac{D\mathbf{u}}{Dt} = -\nabla P$

Mass: $\frac{D\rho}{Dt} + \rho \nabla \cdot \mathbf{u} = 0$

Energy: $\frac{dE}{dt} + P\frac{dV}{dt} = 0$

Hugoniot Equations

Momentum: $P - P_0 = \rho_0 u_p U$

Mass: $\rho\,(U - u_p) = \rho_0 U$

Energy: $E - E_0 = \frac{P+P_0}{2}\left(\frac{1}{\rho_0} - \frac{1}{\rho}\right)$

Conservation of Momentum

Let F = force, m = mass, a = acceleration, A = area, P = pressure, and $\mathbf{u}$ = velocity. From Newton's second law, $F = ma$.

$$P_2 A_2 - P_1 A_1 = m\frac{d\mathbf{u}}{dt}$$

$$-(P_1 A_1 - P_2 A_2) = m\frac{d\mathbf{u}}{dt}$$

$$-\left[\left(P + \frac{dP}{dx}dx\right)A - PA\right] = m\frac{d\mathbf{u}}{dx}\frac{dx}{dt}$$

$$-\frac{dP}{dx}dxA = m\frac{d\mathbf{u}}{dx}\frac{dx}{dt}$$

$$-\frac{dP}{dx} = \rho\mathbf{u}\frac{d\mathbf{u}}{dx} \text{ because } m = \rho dxA$$

$$-\nabla P = \rho\frac{D\mathbf{u}}{Dt} \text{ in Lagrangian form.}$$

https://www.grc.nasa.gov/www/k-12/airplane/conmo.html

Von Mises Effective Stress

Stress tensor: $\begin{bmatrix} \sigma_{11} & \sigma_{12} & \sigma_{13} \\ \sigma_{21} & \sigma_{22} & \sigma_{23} \\ \sigma_{31} & \sigma_{32} & \sigma_{33} \end{bmatrix} = \begin{bmatrix} s_{11} & s_{12} & s_{13} \\ s_{21} & s_{22} & s_{23} \\ s_{31} & s_{32} & s_{33} \end{bmatrix} + \sum \frac{\sigma_{kk}}{3}$

Second invariant: $J_2 = \frac{1}{2}\left(s_{11}^2 + s_{22}^2 + s_{33}^2\right)$

Von Mises flow stress = $\sqrt{3J_2}$

Constitutive Models

Preston-Tonks-Wallace

$$G = G_0\left(1 - \alpha\hat{T}\right)$$

$$\hat{\tau} = \hat{\tau}_s + \frac{1}{p}\left(s_0 - \hat{\tau}_y\right)\ln\left\{1 - \left[1 - \exp\left(-p\frac{\hat{\tau}_s - \hat{\tau}_y}{s_0 - \hat{\tau}_y}\right)\right]\exp\left(-\frac{p\theta\epsilon}{\left(s_0 - \hat{\tau}_y\right)\left[\exp\left(p\frac{\hat{\tau}_s - \hat{\tau}_y}{s_0 - \hat{\tau}_y}\right) - 1\right]}\right)\right\}$$

G: shear modulus (Pa)
G_0: reference shear modulus (Pa)
α: temperature parameter
$\hat{T}$: homologous temperature
$\hat{tau}$: dimensionless stress
$\hat{\tau}_s$: dimensionless work-hardening saturation stress
p: Voce hardening law constant
s_0: dimensionless saturation stress at 0 K
$\hat{\tau}_y$: dimensionless yield stress
θ: initial strain hardening
ϵ: equivalent plastic strain

PTW

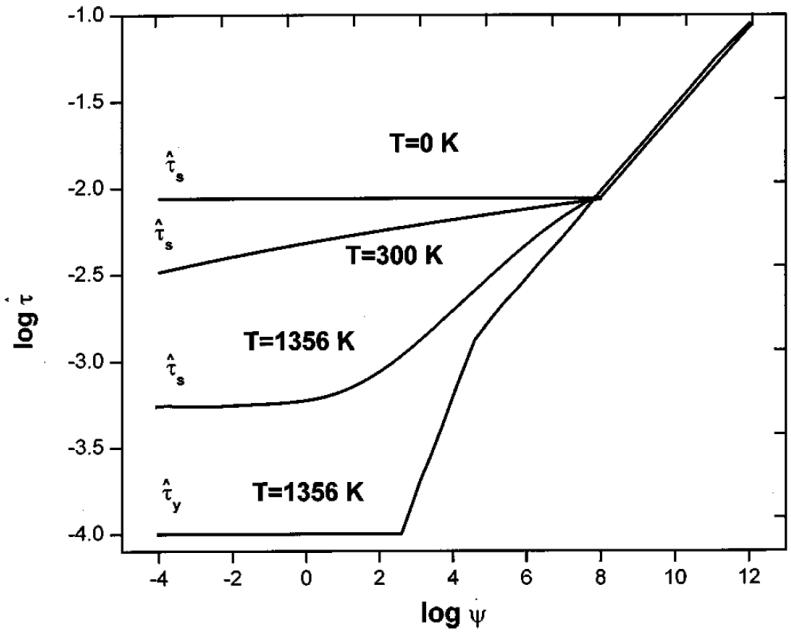

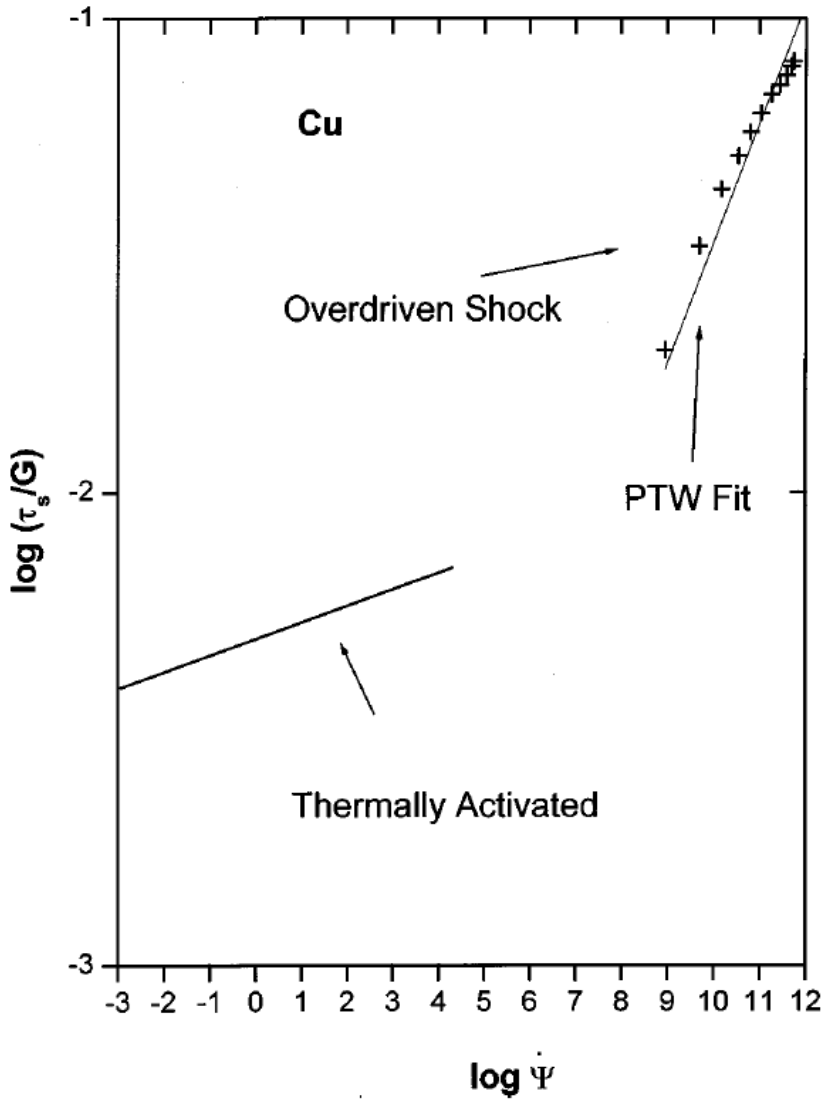

Preston, D. L., D. L. Tonks, and D. C. Wallace. “Model of plastic deformation for extreme loading conditions.” *Journal of Applied Physics* 93(1): 211–220 (2003).

Psyche Setup Simulation Details

2D

- Axisymmetric
- Psyche: Semicircle, 125 km radius
- Impactor: Semcircle, 5 km radius
- Void: Box\(Psyche & Impactor), 500 km x 500 km

3D

- Cartesian
- Psyche: Shape model, spherical cap 110 km radius
- Impactor: Sphere, 5 km radius
- Void: Box\(Psyche & Impactor), 500 km x 500 km

	2D	3D
Zone size min	330 m	1000 m
Zone size max	330 m	10,000 m
Zones	2,301,285	33,382,400
Processors	180	1080
ALE strategy	Eulerian	Eulerian

Psyche Impactor Size

$d_b = L\sqrt{\frac{\rho_I}{\rho_T}}$

Using 1/4 for ρ ratio and $d_b = 5$, $L = 10$ km.

Many other estimates were around 7 km – 12 km.

Melosh, H. J. *Planetary Surface Processes* Vol 13, Cambridge University Press (2011).

Shepard, M. K., J. Richardson, P. A. Taylor, L. A. Rodriguez-Ford, A. Conrad, I. de Pater, M. Adamkovics, K. de Kleer, J. R. Males, K. M. Morzinski *et al*. "Radar observations and shape model of asteroid 16 Psyche," *Icarus* 281: 388–403 (2017).

Crater Formation Time

$$T = 0.8\sqrt{\frac{V^{\frac{1}{3}}}{g}}$$

Largest shape: ellipsoid with 35 km, 6.4 km, and 35 km semi-axes

$$V = \frac{1}{2}\frac{4}{3}\pi(35)(6.4)(35)$$
$$g = 0.29$$
$$T \approx 240 \text{ s}$$

Schmidt, Robert M. and Kevin R. Housen. “Some recent advances in the scaling of impact and explosion cratering.” *International Journal of Impact Engineering* 5(1–4): 543–560, 1987.

Strength vs Gravity

$\pi_2 = \frac{ga}{U^2}$ dominates gravity

$\pi_3 = \frac{Y}{\rho U^2}$ dominates strength

$$\pi_2 = \frac{0.29(5000)}{4500^2} = 7.2E-5$$

$$\pi_3 = \frac{250000000}{8810\,(4500^2)} = 1.4E-3$$

$$\pi_3 > \pi_2$$

Holsapple, Keith A. and Kevin R. Housen. “Craters from Impacts and Explosions,” http://keith.aa.washington.edu/craterdata/scaling/theory.pdf.

Modeling Impact Structures on Asteroid 16 Psyche: 3D

Crater	Dimension			6.4 ± 0.64 km[†]	67 ± 15 km[†]
Impactor	Psyche	Porosity	Angle	Depth	Diameter
Monel	Monel	Solid	45º	**7 km**	35.1438 km
Monel	Monel	Solid	60º	5.3 km	36.8 km
SiO_2	Monel	Solid	45º	0.1 km	41.0122 km
SiO_2	Monel	Solid	60º	1.1 m	28.5 km
Monel	Monel	30%	45º	5.5 km	39.598 km
Monel	Monel	30%	60º	10.4 km	*51.5 km*
Monel	Monel	50%	45º	14.5 km	42.4264 km
Monel	Monel	50%	60º	12 km	**60 km**

Table: FLAG simulation results from 3D oblique impacts. **Bold** results indicate values that lie within the error bars of the actual crater dimensions. *Italic* results indicate values that lie within the error bars after correct for the expected numerical error based on the glass-water validation problem.

[†] Shepard, M. K., J. Richardson, P. A. Taylor, L. A. Rodriguez-Ford, A. Conrad, I. de Pater, M. Adamkovics, K. de Kleer, J. R. Males, K. M. Morzinski *et al*. "Radar observations and shape model of asteroid 16 Psyche," *Icarus* 281:388–403 (2017).